Report No. UT-26.11

DURABILITY OF RAPID-SETTING CONCRETE REPAIRS ON PAVEMENT PANELS AND BRIDGE DECKS IN UTAH

Prepared For:

Utah Department of Transportation
Research & Innovation Division

Final Report
February 2026

RESEARCH

UDOT
Keeping Utah Moving

Utah Department of Transportation - Research Division
4501 South 2700 West - P.O. Box 148410 - SLC,UT 84114-8410

DISCLAIMER

The authors alone are responsible for the preparation and accuracy of the information, data, analysis, discussions, recommendations, and conclusions presented herein. The contents do not necessarily reflect the views, opinions, endorsements, or policies of the Utah Department of Transportation (UDOT) or the U.S. Department of Transportation. UDOT makes no representation or warranty of any kind, and assumes no liability therefore. The authors also make no warranty, express or implied, regarding the suitability of findings documented in this report for a particular purpose and shall not be held liable under any circumstances for any direct, consequential, or other damages with respect to claims by users of any findings documented in this report, including claims based on allegations of errors, omissions, or negligence.

ACKNOWLEDGMENTS

Funding for this research was provided through UDOT and the King Husein Professorship within the Department of Civil and Construction Engineering at Brigham Young University (BYU). The patching material used for field work performed in this research was donated by CTS Cement Corporation. Assistance with field and laboratory work was provided by Dr. Robert Stevens and Adam Guthrie of Infrastructure Research and Jaron Hamblin of BYU. Patrick McDivitt of BYU assisted with the literature review.

TECHNICAL REPORT ABSTRACT

1. Report No.	2. Government Accession No.	3. Recipient's Catalog No.
UT- 26.11	N/A	N/A

4. Title and Subtitle	5. Report Date / 6. Performing Organization Code
Durability of Rapid-Setting Concrete Repairs on Pavement Panels and Bridge Decks in Utah	5. Report Date: February 2026 6. Performing Organization Code: N/A
7. Author(s) W. Spencer Guthrie, Ph.D., Steven B. Burdette, Lorenzo Eusebi-Diehr	8. Performing Organization Report No. N/A
9. Performing Organization Name and Address Brigham Young University Department of Construction and Civil Engineering 368 Clyde Building Provo, UT 84604	10. Work Unit No. 5H094 05H 11. Contract or Grant No. 23-8052
12. Sponsoring Agency Name and Address Utah Department of Transportation 4501 South 2700 West P.O. Box 148410 Salt Lake City, UT 84114-8410	13. Type of Report & Period Covered Final July 2022 to February 2026 14. Sponsoring Agency Code PIC No. UT20.106

15. Supplementary Notes

Prepared in cooperation with the Utah Department of Transportation and the U.S. Department of Transportation, Federal Highway Administration

16. Abstract

The objective of this research was to evaluate the durability of rapid-setting concrete batched using volumetric concrete mixers and placed in a cold region. The scope of work included field and laboratory evaluations of rapid-setting concrete repairs on both pavement panels and bridge decks in Utah. Six sites in northern Utah were selected by Utah Department of Transportation (UDOT) personnel for evaluation. At the time of inspection, the repairs had been in service for 4 to 5 years.

Regarding field research, cracking and scaling were observed to be the most prevalent distresses among the sites evaluated in this research. Schmidt rebound numbers ranged from 40 to 55, which corresponds to a range of 5500 to 8700 psi, and all resistivity values correspond to a corrosion potential classification of "low."

Regarding laboratory research, stiffness values ranged from 3647 to 5431 ksi. All compressive strength values, which ranged from 5213 to 10867 psi, exceeded the minimum compressive strength of 5200 psi required by UDOT. Splitting tensile strength values ranged from 642 to 864 psi. Rapid chloride permeability test values corresponded to classifications of "negligible" or "very low," and the absorption values of these specimens ranged from 7.5 to 9.9 percent. The hardened air void analyses indicated total air contents ranging from 4.6 to 11.9 percent, where the lowest and highest total air contents are outside the limits specified by UDOT, and microscope photographs suggest improper finishing practices and inadequate surface curing for those cores. The chloride concentrations, generally decreasing with increasing depth, ranged from less than 0.1 to 12.8 lb Cl^-/yd^3 of concrete within the upper 4 in. With recommended improvements in mixture design, finishing, and curing, rapid-setting concrete batched using volumetric concrete mixers should continue to be used for repairs of concrete pavement panels and bridge decks in Utah to expedite the concrete curing process and thereby minimize the impacts of lane closures on traffic.

17. Key Words	18. Distribution Statement	23. Registrant's Seal
Calcium sulfoaluminate cement, concrete bridge deck, durability, patching, pavement panel, rapid-setting concrete, volumetric mixer truck	Not restricted. Available through: UDOT Research & Innovation Div. 4501 South 2700 West P.O. Box 148410 Salt Lake City, UT 84114-8410 www.udot.utah.gov/go/research	N/A

19. Security Classification (of this report)	20. Security Classification (of this page)	21. No. of Pages	22. Price
Unclassified	Unclassified	109	N/A

TABLE OF CONTENTS

LIST OF TABLES

LIST OF FIGURES

LIST OF ACRONYMS

ASTM	American Society for Testing and Materials
BYU	Brigham Young University
CSA	calcium sulfoaluminate
RCPT	rapid chloride permeability test
UDOT	Utah Department of Transportation

EXECUTIVE SUMMARY

The objective of this research was to evaluate the durability of rapid-setting concrete batched using volumetric concrete mixers and placed in a cold region. The scope of work included field and laboratory evaluations of rapid-setting concrete repairs on both pavement panels and bridge decks in Utah. Six sites in northern Utah were selected by Utah Department of Transportation (UDOT) personnel for evaluation. At the time of inspection, the repairs had been in service for 4 to 5 years. Field research included visual inspection, Schmidt rebound hammer testing, resistivity testing, and concrete sampling. Laboratory research included stiffness testing, compressive strength testing, splitting tensile strength testing, rapid chloride permeability testing, absorption measurements, hardened air void analyses, and chloride concentration analyses.

The results are expected to be applicable to rapid-setting concrete repairs with similar concrete mixture designs, construction practices, and service conditions as those studied in this research. Regarding field research, cracking and scaling were observed to be the most prevalent distresses among the sites evaluated in this research. Schmidt rebound numbers ranged from 40 to 55, which corresponds to a range of 5500 to 8700 psi, and all resistivity values correspond to a corrosion potential classification of "low."

Regarding laboratory research, stiffness values ranged from 3647 to 5431 ksi. All compressive strength values, which ranged from 5213 to 10867 psi, exceeded the minimum compressive strength of 5200 psi required by UDOT. Splitting tensile strength values ranged from 642 to 864 psi. Rapid chloride permeability test values corresponded to classifications of "negligible" or "very low," and the absorption values of these specimens ranged from 7.5 to 9.9 percent. The hardened air void analyses indicated total air contents ranging from 4.6 to 11.9 percent, where the lowest and highest total air contents are outside the limits specified by UDOT, and microscope photographs suggest improper finishing practices and inadequate surface curing for those cores. The chloride concentration analyses showed that, in general, chloride concentration decreases with increasing depth, and, overall, chloride concentrations ranged from less than 0.1 to 12.8 lb Cl^-/yd^3 of concrete within the upper 4 in. With recommended improvements in mixture design, finishing, and curing, rapid-setting concrete batched using volumetric concrete mixers should continue to be used for repairs of concrete pavement panels and bridge decks in Utah to expedite the concrete curing process and thereby minimize the impacts of lane closures on traffic.

1.0 INTRODUCTION

1.1 Problem Statement

Repairs of concrete pavement panels and bridge decks in Utah are commonly performed using rapid-setting concrete to expedite the concrete curing process and thereby minimize the impacts of lane closures on traffic. The use of rapid-setting concrete, which can be manually batched from prepackaged bags for smaller repairs or batched using volumetric concrete mixers (Edwards et al., 2018; Priddy et al., 2016; UDOT, 2024c) for larger repairs, allows the affected lanes to be re-opened to traffic within just hours after repair. One such concrete repair product exhibits final set in just 35 minutes and can reach a compressive strength of 3000 psi in less than 2 hours (CTS Cement Manufacturing Corporation, 2025), while another product exhibits final set in 20 minutes and can reach a compressive strength of 4500 psi in 1.5 hours (CTS Cement Manufacturing Corporation, 2023). Yet another product has supported aircraft loading in as little as 2 hours after placement (Edwards et al., 2018; Priddy et al., 2016). Compressive strengths of 5550 psi after 1 hour (de Bruyn et al., 2017) and 3190 and 5220 psi after 1 day (Moffatt and Thomas, 2018) have also been reported.

Although a satisfactory strength can be readily achieved, the durability of rapid-setting concrete is a concern in especially cold regions such as northern Utah, where exposure to moisture, freezing, deicing salts, and snowplows can be problematic. Specifically, information about the durability of rapid-setting concrete placed on both pavement panels and bridge decks in Utah was needed. The Utah Department of Transportation (UDOT) therefore commissioned this study to evaluate the durability of rapid-setting concrete batched using volumetric concrete mixers and placed at several sites in Utah.

1.2 Research Objective and Scope of Work

The objective of this research was to evaluate the durability of rapid-setting concrete batched using volumetric concrete mixers and placed in a cold region. The scope of work included field and laboratory evaluations of rapid-setting concrete repairs on both pavement panels and bridge decks in Utah. Six sites in northern Utah that were repaired in 2018 or 2019 when UDOT was transitioning to more frequent use of rapid-setting concrete batched using volumetric concrete mixers were selected for evaluation. Field research at these sites included distress surveys, Schmidt rebound hammer testing, resistivity testing, and concrete sampling. Laboratory research, which was performed on samples removed from the test sites, included stiffness testing, compressive strength testing, splitting tensile strength testing, rapid chloride permeability testing, absorption measurements, hardened air void analyses, and chloride concentration analyses.

1.3 Report Outline

This report consists of five chapters. Chapter 1 provides an introduction, and Chapter 2 discusses relevant background information obtained primarily from a literature review. Chapter 3 explains the field and laboratory testing procedures, and Chapter 4 presents the results of the research. Finally, Chapter 5 offers conclusions and recommendations based on the research findings.

2.0 BACKGROUND

2.1 Overview

Background information obtained from a literature review is provided on rapid-setting concrete mixture design, rapid-setting concrete repairs, damage mechanisms, and rapid-setting concrete durability as described in the following sections.

2.2 Rapid-Setting Concrete Mixture Design

Design of rapid-setting concrete mixtures for in-field repairs requires consideration of binders, aggregates, and admixtures. The type and quantity of each of these ingredients influence the subsequent performance of the repairs.

One binder commonly used in rapid-setting concrete mixtures is calcium sulfoaluminate (CSA) cement (de Bruyn et al., 2017; Guo et al., 2014; Moffatt, 2016; Moffatt and Thomas, 2018; Zhang et al., 2020). CSA cement comprises relatively high amounts of alumina, which reacts rapidly with water to form ettringite (de Bruyn et al., 2017; Mindess et al., 2003). Indeed, consuming much of the available water in the concrete mixture, early-forming ettringite reduces water bleeding in the fresh concrete and thereby also reduces both the permeability and shrinkage of the hardened concrete (Guo et al., 2014). Early formation of ettringite, which is a hexagonal crystalline compound (Mindess et al., 2003; Moffatt, 2016) illustrated in Figure 2.1 (Jewell et al., 2015), is critical to facilitate rapid set and strength gain of concrete mixtures comprising CSA cement (de Bruyn et al., 2017; Moffatt, 2016; Moffatt and Thomas, 2018). Strength is gained as ettringite grows into the capillary pores between cement grains (Mindess et al., 2003). To achieve typical strengths required for concrete pavement panels and bridge decks, a range of 611 to 799 lbs. of CSA cement per cubic yard of concrete is commonly specified, which equates to 6.5-bag to 8.5-bag mixtures. Mixtures with higher binder contents may exhibit higher strength but may also exhibit brittle behavior, which can lead to cracking (Mindess et al., 2003).

The chemical and physical properties of aggregates used to produce rapid-setting concrete mixtures are important because aggregate comprises a comparatively high percentage of the volume of concrete and thus heavily influences its overall strength and durability. Regarding chemical properties, aggregates that are not susceptible to deleterious alkali-silica or alkali-

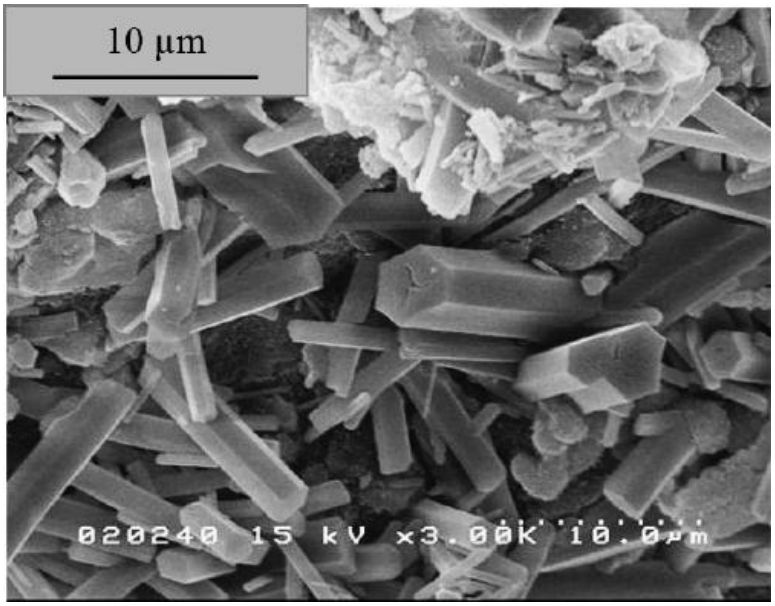

Figure 2.1 Scanning electron microscope image of ettringite crystals within a calcium sulfoaluminate-belite paste (Jewell et al., 2015).

carbonate reactions should be specified, and aggregates must also be free of impurities, such as organic compounds, that can negatively affect the setting of cement (Mindess et al., 2003). Regarding physical properties, sound aggregates that do not experience changes in volume with freeze-thaw and/or wet-dry cycles or absorb high amounts of water should be specified to avoid premature concrete deterioration, and aggregates must also be hard, dense, and strong to provide resistance to abrasion and wear (Mindess et al., 2003). The nominal maximum aggregate size should be limited to a value that allows proper consolidation of the concrete into the repair area; in Utah, the nominal maximum aggregate size for rapid-setting concrete used to repair pavement panels and bridge decks is limited to 0.75 in. and 0.375 in., respectively, as the presence of reinforcing steel in bridge decks requires smaller aggregate (UDOT, 2024b; UDOT, 2024c).

Admixtures may be included in rapid-setting concrete mixtures to optimize performance. Air-entraining admixtures are added to typical mixtures requiring resistance to freeze-thaw damage, which is an important consideration in cold regions. UDOT specifies that rapid-setting concrete mixtures should have an air content between 5.0 and 7.5 percent (UDOT, 2024c). Although the degree of air entrainment can be measured as described in American Society for

Testing and Materials (ASTM) C231 (Standard Test Method for Air Content of Freshly Mixed Concrete by the Pressure Method), some agencies, including UDOT, have not required contractors to perform this test due to the risk that the concrete may harden inside the testing apparatus. Water-reducing admixtures, which can be added to improve the workability of concrete, are commonly required when a low water-cementitious materials ratio is specified. Finally, set-retarding admixtures can be added to slow cement hydration.

2.3 Rapid-Setting Concrete Repairs

Rapid-setting concrete incorporating CSA cement is often preferred over conventional Portland cement concrete for repairs of concrete pavement panels and bridge decks on high-traffic facilities. While conventional concrete can require several days of curing to achieve the minimum strength required for traffic (UDOT, 2024a; UDOT, 2024d), rapid-setting concrete can be opened to traffic just hours after placement. Use of rapid-setting concrete can therefore eliminate extended lane closures and the corresponding agency and user costs (Mallela and Sadasivam, 2011; Moffatt, 2016; Moffatt and Thomas, 2018).

Rapid-setting concrete can be used for both partial-depth and full-depth repairs of pavement panels and bridge decks, which may exhibit distresses such as cracking, scaling, spalling, or delamination, for example (Huang, 2004; Miller and Bellinger, 2003). Following saw-cutting, jackhammering, and removal of the damaged concrete, the edges and bottom of the repair area are cleaned and pre-wetted, often using chilled water applied using a pressure washer. For larger repairs, rapid-setting concrete is then batched on site using a volumetric concrete mixer, depicted in Figure 2.2, which can produce fresh concrete on demand using on-board materials. The materials are simultaneously dispensed from separate containers and mixed using an auger for several seconds before exiting the mixer through a chute. Although a 45-degree angle is typically recommended for the auger chute of a volumetric concrete mixer, American Concrete Institute 304.6R (Guide for the Use of Volumetric-Measuring and Continuous-Mixing Concrete Equipment) suggests that the performance of admixtures, in particular, can be improved by increasing the mixing time by increasing the upward angle of the mixing auger. Because this product sets quickly, construction personnel must immediately place, consolidate, and finish the concrete while avoiding errors that may not be correctable after the concrete hardens. Beyond adequately smoothing the surface of the concrete, avoiding over-finishing and implementing proper curing practices are important to minimize cracking (Edwards et al., 2018;

Figure 2.2 Volumetric concrete mixer.

Moffatt and Thomas, 2018). Curing practices may involve application of poly alpha-methylstyrene (PAMS) or pre-soaked burlap, for example.

2.4 Damage Mechanisms

Once in service, rapid-setting concrete repairs on a pavement panel or bridge deck are subject to traffic loading and environmental conditions that can lead to concrete damage (Huang, 2004) such as cracking, scaling, spalling, or delamination (Huang, 2004; Miller and Bellinger, 2003). Generally, concrete cracks when its tensile strength is exceeded by an induced tensile stress associated with traffic loads, drying shrinkage, or temperature-induced contraction (Mindess et al., 2003). Scaling of the concrete may occur if water or salt is able to penetrate the surface and subsequently freeze or precipitate, respectively; the corresponding volume expansion of ice or precipitating salt causes the concrete surface to flake off, leaving a rough texture (Miller and Bellinger, 2003). More extensive damage in the form of spalling can also occur, especially at joints where water ingress is more prevalent and where the concrete repair may be more exposed to impacts from traffic loads and snowplows (Guthrie et al., 2005). Delamination and subsequent spalling are possible in partial-depth repairs when the bond between the concrete repair and the underlying concrete fails, causing the repair to become detached (Stevens et al., 2021). Delamination may also occur when chloride-induced corrosion of reinforcing steel that is embedded in or present under the concrete repair leads to expansion of the steel and subsequent subsurface cracking within the concrete (Hendricks et al., 2020; Moffatt and Thomas, 2018). The durability of rapid-setting concrete depends on its ability to resist such damage under the traffic loading and environmental conditions present at a given site over time.

2.5 Rapid-Setting Concrete Durability

Previous evaluations of rapid-setting concrete durability have generally been limited to freeze-thaw cycling, chloride ingress, and carbonation. One laboratory study indicated that a concrete mixture comprising CSA cement and freeze-thaw-susceptible aggregate performed better than a concrete mixture comprising Portland cement and the same aggregate when subjected to freeze-thaw cycling in general accordance with ASTM C666 (Standard Test Method for Resistance of Concrete to Rapid Freezing and Thawing) (de Bruyn et al., 2017); the former sustained three times as many cycles as the latter before the failure criteria were met. The study also reported that a concrete mixture comprising CSA cement and durable aggregate sustained 11 percent less mass loss than a concrete mixture comprising Portland cement and the same aggregate, again when tested using ASTM C666 (de Bruyn et al., 2017). However, another study, which included both field and laboratory components (Moffatt and Thomas, 2018), provided conflicting results for laboratory and field evaluations of salt scaling in freeze-thaw conditions. In the laboratory, a concrete mixture comprising one blend of CSA cement performed better than a concrete mixture comprising Portland cement, but another concrete mixture comprising a different blend of CSA cement performed worse; in the field, the concrete mixture comprising Portland cement performed better than both of the concrete mixtures comprising blends of CSA cement (Moffatt and Thomas, 2018).

Regarding chloride ingress, one study reported lower chloride diffusion coefficients for concrete comprising CSA cement than for concrete comprising Portland cement (Zhao et al., 2014). Another study indicated that a concrete mixture comprising a blend of CSA cement exhibited higher chloride permeability than other rapid-setting and Portland cement concrete mixtures according to a bulk chloride diffusion test conducted in general accordance with ASTM

C1556 (Standard Test Method for Determining the Apparent Chloride Diffusion Coefficient of Cementitious Mixtures by Bulk Diffusion), but the opposite was indicated by a rapid chloride permeability test (RCPT) conducted in general accordance with ASTM C1202 (Standard Test Method for Electrical Indication of Concrete's Ability to Resist Chloride Ion Penetration) (Moffatt and Thomas, 2018).

Carbonation, which can lead to corrosion of reinforcing steel in concrete (Mindess et al., 2003), was shown in one study to occur at a faster rate in concrete comprising CSA cement than in concrete mixtures comprising only Portland cement (Moffatt and Thomas, 2018). In the same study, a chloride-ponding experiment also showed that reinforcing steel embedded in a concrete mixture comprising a blend of CSA cement exhibited a high amount of corrosion after 8 weeks while other concrete mixtures, including one comprising a blend of CSA and Portland cement and multiple comprising strictly Portland cement, exhibited low or intermediate amounts of corrosion (Moffatt and Thomas, 2018). However, the results of a different study indicated that mortars comprising CSA cement generally exhibited less carbonation than mortar comprised of a composite cement including Portland clinker, gypsum, limestone, and granulated blast furnace slag (Cemmac, 2018; Guo et al., 2014).

This conflicting and limited information from the literature warrants additional research focused on the durability of rapid-setting concrete. Specifically, further research related to the durability of field placements of rapid-setting concrete is needed.

2.6 Summary

Design of rapid-setting concrete mixtures for in-field repairs requires consideration of binders, aggregates, and admixtures. Early formation of ettringite, which is a hexagonal crystalline compound, is critical to facilitate rapid set and strength gain of concrete mixtures comprising CSA cement, which is a binder commonly used in rapid-setting concrete mixtures. Aggregates that are not susceptible to deleterious reactions and are free of impurities, sound, hard, dense, and strong should be specified, and the nominal maximum aggregate size should be limited to a value that allows proper consolidation of the concrete into the repair area. Admixtures may be included in rapid-setting concrete mixtures to optimize performance.

While conventional concrete can require several days of curing to achieve the minimum strength required for traffic, rapid-setting concrete can be opened to traffic just hours after placement. Rapid-setting concrete can be used for both partial-depth and full-depth repairs of pavement panels and bridge decks. For larger repairs, rapid-setting concrete is then batched on site using a volumetric concrete mixer, which can produce fresh concrete on demand using on-board materials. Because this product sets quickly, construction personnel must immediately place, consolidate, and finish the concrete while avoiding errors that may not be correctable after the concrete hardens. Beyond adequately smoothing the surface of the concrete, avoiding over-finishing and implementing proper curing practices are important to minimize cracking.

Once in service, rapid-setting concrete repairs on a pavement panel or bridge deck are subject to traffic loading and environmental conditions that can lead to concrete damage such as cracking, scaling, spalling, or delamination. The durability of rapid-setting concrete depends on its ability to resist such damage under the traffic loading and environmental conditions present at a given site over time.

Previous evaluations of rapid-setting concrete durability have generally been limited to freeze-thaw cycling, chloride ingress, and carbonation. The conflicting and limited information from the literature warrants additional research focused on the durability of rapid-setting concrete. Specifically, further research related to the durability of field placements of rapid-setting concrete is needed.

3.0 PROCEDURES

3.1 Overview

The scope of work included both field and laboratory research. The following sites in northern Utah were selected by UDOT personnel for evaluation: 1) southbound Interstate 215 (I-215) at exit 21, 2) eastbound State Route 201 (SR-201) at 4000 West, 3) westbound SR-201 at Surplus Canal, 4) eastbound Interstate 80 (I-80) at exit 115A, 5) northbound U.S. Highway 40 (US-40) at the I-80 interchange, and 6) northbound Interstate 15 (I-15) at 1700 South, as shown in Figure 3.1. These six sites, which were among many potential sites having rapid-setting concrete repairs, were selected by UDOT personnel to include representative types of repairs installed by different contractors on facilities that could be approved for lane closures. Rapid-setting concrete repairs were placed at these sites during 2018 or 2019 by two different contractors, and each site was inspected in 2023. Thus, at the time of inspection, the repairs had been in service for 4 to 5 years. The repair type, defined as pavement panel, approach slab, or bridge deck, is given in Table 3.1 for each site.

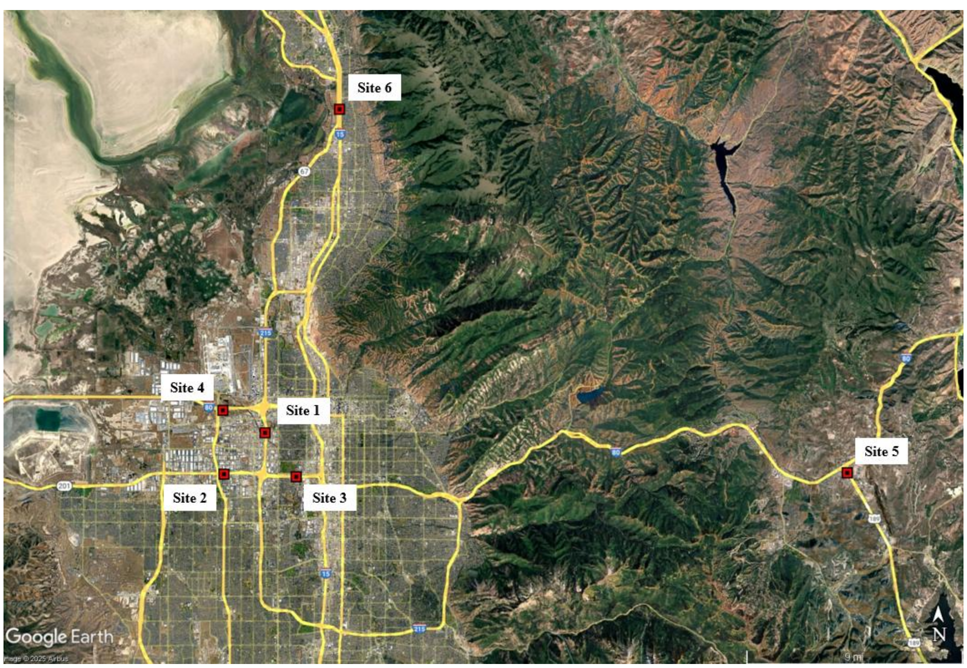

Figure 3.1 Site locations.

Table 3.1 Site Information

Site	Main Line	Interchange	Repair Type
1	I-215	Exit 21	Pavement panel
2	SR-201	4000 West	Pavement panel
3	SR-201	Surplus Canal	Approach slab
4	I-80	Exit 115 A	Bridge deck
5	US-40	I-80	Pavement panel
6	I-15	1700 South	Pavement panel

3.2 Field Research

To facilitate the field research, which occurred during July and August 2023, a portion of each site was closed to traffic, generally in the evening or at night, and the individual rapid-setting concrete repairs were then numbered relative to a predetermined origin for labeling purposes; some repairs were subdivided because they were overly large or irregular in shape. In general, the numbering of the repairs increased transversely from left to right, with respect to the direction of traffic flow, and longitudinally in the direction of traffic flow. At bridge facilities where repairs of sufficient size were present on bridge decks, approach slabs, and the adjacent pavement panels, repairs in only one of these locations were evaluated, given that different mixture designs may have been used in these different applications. Table 3.2 shows the quantity of numbered repairs at each site.

At each site, three or four repairs were then selected for evaluation. If any of the repairs exhibited a noticeably higher severity of material-related distress than the other repairs, the repair with the most severe distress was manually selected first, as requested by UDOT personnel, to ensure that distressed repairs would be included in the study. Afterward, three additional repairs

Table 3.2 Numbered Repairs by Site

Site	Numbered Repairs
1	15
2	5
3	4
4	29
5	4
6	20

were then selected for evaluation using a formal random sampling procedure, which ensured that each repair had an equal chance of being selected and that the resulting selection would therefore be as representative of the site as possible. If none of the repairs exhibited more severe material-related distress than the other repairs, only three repairs were randomly selected at the site. A distress survey of each repair was then performed.

For Schmidt rebound hammer testing, resistivity testing, and concrete sampling, the specific location to be tested within each repair was marked following a predetermined procedure to ensure that corners, centers, and edges of repairs would be evaluated. Based on the order in which the randomly selected repairs were selected, the first repair was tested in the downstream right corner, the second repair was tested in the center, and the third repair was tested in the middle of the upstream edge. Repairs that were manually selected because they exhibited a noticeably higher severity of material-related distress than the other repairs were generally tested directly in the area of highest distress. At each test location, testing and sampling were generally performed within an approximately 1-ft by 1-ft square following the predetermined layout presented in Figure 3.2 and depicted in Figure 3.3. Minor adjustments were made to the testing location and/or testing layout in some cases to avoid testing directly on lane markings or coring through cracks or into embedded steel reinforcement, which was detected on the bridge deck and approach slab using a cover meter as shown in Figure 3.4; in general, testing was performed at least 2 ft from the edges of panels and slabs, to avoid tie bars and dowels, and between longitudinal and transverse bars on the bridge deck. A No. 5 bar size was assumed for cover depth testing.

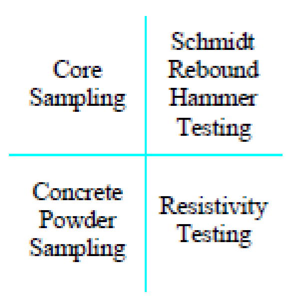

Figure 3.2 Schematic of typical testing layout.

Figure 3.3 Example testing layout.

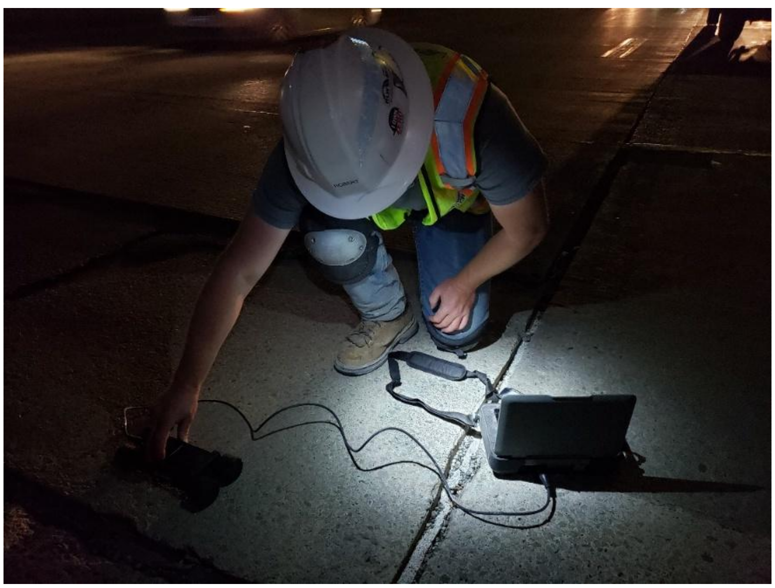

Figure 3.4 Cover depth testing.

3.2.1 Distress Surveys

As illustrated in Figure 3.5, manual measurements of each observed distress were performed in general accordance with Federal Highway Administration guidelines (Miller and Bellinger, 2003) to prepare a distress map, or drawing, of each selected repair, including the locations and/or extent of cracks, scaling, and spalling. Crack widths were estimated using a

Figure 3.5 Distress measurements.

crack comparator card, with multiple measurements being recorded along cracks that clearly exhibited varying width. Chain dragging was performed to identify the occurrence of delamination, which was also mapped. Finally, distresses that were presumed to be the result of construction-related issues were noted. Photographs were taken to aid in data analysis, including, for example, quantifying the extent of scaling and estimating the locations of lane striping. As needed, work lights were used to illuminate the inspected repairs. Concrete surfaces appeared to be dry during visual inspection.

Following data collection, the drawings were scanned and subsequently digitized using computer-aided drafting software. Crack lengths and widths and areas of scaling, spalling, and delamination, as well as the total area of each selected repair, were tabulated. Crack density was then calculated by dividing the total length of cracks in a given repair by the area of that repair, and the average crack width for a given repair was calculated by weighting the width of each crack by its length, where cracks with different widths were discretized into shorter cracks of approximately constant width. Area densities for scaling, spalling, delamination, and construction-related issues for each repair were calculated by dividing the measured area of the given distress by the area of the repair.

3.2.2 Schmidt Rebound Hammer Testing

Schmidt rebound hammer testing was performed in general accordance with ASTM C805 (Standard Test Method for Rebound Number of Hardened Concrete). Prior to testing, an angle grinder equipped with a masonry grinding wheel was used to smooth the concrete surface. As depicted in Figure 3.6, Schmidt rebound hammer testing was then performed between tines, if present, and between any visible coarse aggregate particles. Five Schmidt rebound hammer tests were performed at each location, and the average of the middle three numbers was reported as the Schmidt rebound number for the given location.

3.2.3 Resistivity Testing

Resistivity testing was performed using a two-prong probe (Barrus, 2012). At each test location, two sets of holes were drilled approximately 1.5 in. apart, where a set included two 0.25-in.-diameter holes spaced 2.0 in. apart to match the prong positions. Each of the four holes

Figure 3.6 Schmidt rebound hammer testing.

was drilled to a depth of approximately 0.5 in. After the holes were cleaned using compressed air, several drops of a conductive solution were added to each hole. The probe was then inserted into each set of holes as shown in Figure 3.7, and the resistivity was measured. The probe was then rotated end for end, and the resistivity was measured again. The surface temperature of the concrete at each test location was also measured using a spot radiometer.

3.2.4 Concrete Sampling

Concrete sampling included collection of concrete powder and concrete cores for laboratory testing. Concrete powder sampling was performed using carbide-tipped rotary hammer bits in four 1-inch-depth intervals at each test location. To minimize contamination of samples obtained from deeper intervals by inadvertent scraping of the inside of the hole nearer the surface, smaller bits were used with increasing depth, as shown in Table 3.3. After each depth interval was drilled, the resulting concrete powder was collected using a small scoop

Figure 3.7 Resistivity testing.

Table 3.3 Bit Sizes Used for Concrete Powder Sampling

Lift	Sampling Depth (in.)	Drill Bit Diameter (in.)
1	0 to 1	1.75
2	1 to 2	1.50
3	2 to 3	1.38
4	3 to 4	1.25

as depicted in Figure 3.8, sealed in a plastic bag, and labeled. The hole, drill bit, scoop and other tools were then cleaned using a vacuum and/or compressed air before the next depth interval was drilled.

Coring was performed through intact concrete, confirmed using chain dragging, at each test location using a 4-inch-diameter core bit as depicted in Figure 3.9. For pavement panels, the target depth of coring was the full depth of the panel, while, for bridge decks, the target depth of coring was 5.5 in. Where applicable, cores that remained attached to the underlying concrete were broken loose with a screwdriver and hammer. After being extracted from the hole with a core-removal tool, each core was then dried with a towel, enclosed in plastic wrap and aluminum foil, and labeled.

After the concrete powder sampling and coring were completed, any remaining powder and/or water was removed from the holes. Air-entrained rapid-setting concrete was then manually batched on site, as shown in Figure 3.10, consolidated into the holes using a 0.375-in.-diameter rod, and subsequently leveled using a magnesium float.

Figure 3.8 Concrete powder sampling.

Figure 3.9 Coring.

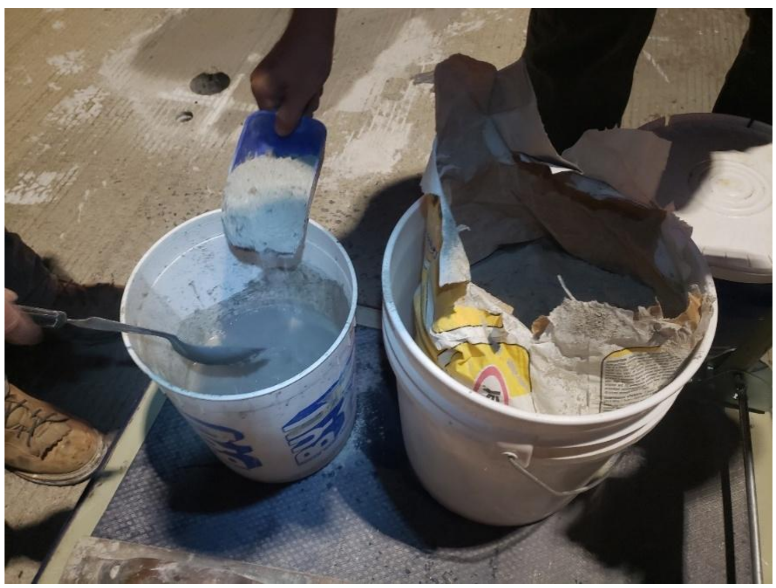

Figure 3.10 Concrete patching.

3.3 Laboratory Research

Laboratory research, which was performed on samples removed from the test sites, included stiffness testing, compressive strength testing, splitting tensile strength testing, rapid chloride permeability testing, absorption measurements, hardened air void analyses, and chloride concentration analyses. After the top and/or bottom of the cores was trimmed as needed to provide flat surfaces, the unit weight and stiffness of each concrete core was measured. Based on the lengths of the cores, a plan was developed for additional laboratory testing procedures. In general, the longest cores were reserved for compressive strength testing, and other cores with sufficient length were cut into two pieces to facilitate additional tests. Lower portions of cut cores were used for rapid chloride permeability testing and absorption measurements, as they were expected to have had a lower previous exposure to chloride ions. Upper portions of cut cores, as well as short cores not suitable for cutting into two pieces, were used for other tests, including splitting tensile strength testing and hardened air void analyses.

3.3.1 Stiffness Testing

Stiffness testing of the core samples was performed in general accordance with ASTM C215 (Standard Test Method for Fundamental Transverse, Longitudinal, and Torsional Frequencies of Concrete Specimens). Cores were tested in the vertical orientation, with the accelerometer mounted to one end of the core and a hammer impact being applied to the other end of the core as illustrated in Figure 3.11. The test controller indicated the resonant frequency for each core, which was used to calculate Young's modulus as shown in Equation 3.1.

$$E = \frac{\frac{\gamma}{32.2}(2lf)^2}{144} \qquad (3.1)$$

where E = Young's modulus, psi

γ = density of the specimen, pcf

l = length of the specimen, ft

f = resonant frequency of the specimen, Hz

3.3.2 Compressive Strength Testing

Compressive strength testing of selected core samples was performed in general accordance with ASTM C39 (Standard Test Method for Compressive Strength of Cylindrical Concrete Specimens). The ends of the cores were capped using neoprene pads mounted in steel retainers, as shown in Figure 3.12, and the load was applied at a target strain rate of 0.05

Figure 3.11 Stiffness testing.

Figure 3.12 Compressive strength testing.

in./minute until failure. The compressive strength was determined by dividing the load at failure by the initial cross-sectional area of the core. Strength correction factors published in ASTM C42 (Standard Test Method for Obtaining and Testing Drilled Cores and Sawed Beams of Concrete) and duplicated in Table 3.4 were utilized when the ratio of the length to the diameter of a core was less than or equal to 1.75; as needed, linear interpolation was used to obtain values for specific ratios.

3.3.3 Splitting Tensile Strength Testing

Splitting tensile strength testing of selected core samples was performed in general accordance with ASTM C496 (Standard Test Method for Splitting Tensile Strength of Cylindrical Concrete Specimens). As shown in Figure 3.13, a diameter was pre-marked across one end of each core to aid in the placement of thin wooden bearing strips, and the load was applied at a target strain rate of 0.05 in./minute. The compressive load that resulted in splitting of the concrete specimens was recorded and used to calculate the splitting tensile strength as shown in Equation 3.2 (Mindess et al., 2003).

$$\sigma_t = \frac{2P}{\pi L D} \qquad (3.2)$$

where σ_t = splitting tensile strength, psi

P = applied compressive load, lb

L = cylinder length, in.

D = cylinder diameter, in.

Table 3.4 Correction Factors for Compressive Strength Test Results

Ratio of Length to Diameter	Correction Factor
1.75	0.98
1.50	0.96
1.25	0.93
1.00	0.87

Figure 3.13 Splitting tensile strength testing.

3.3.4 Rapid Chloride Permeability Testing and Absorption Measurements

RCPTs were performed on selected cores in general accordance with ASTM C1202. The lower portion of each core, which was expected to have had a lower previous exposure to chloride ions, was trimmed to a target height of 2.0 in. for testing. The resulting samples were vacuum saturated and then tested as illustrated in Figure 3.14. At the conclusion of the 6-hour test, the test controller indicated the total number of coulombs that passed through the sample, as well as the corresponding chloride permeability category.

Absorption measurements were performed in conjunction with RCPTs. Immediately following the vacuum-saturation process required for the RCPT, each soaked sample was dried with a towel and weighed. After the RCPT was completed, each sample was dried to constant weight in an oven, as shown in Figure 3.15, at 230°F and then weighed again. Absorption values were computed based on the absorbed water weight and the dry sample weight.

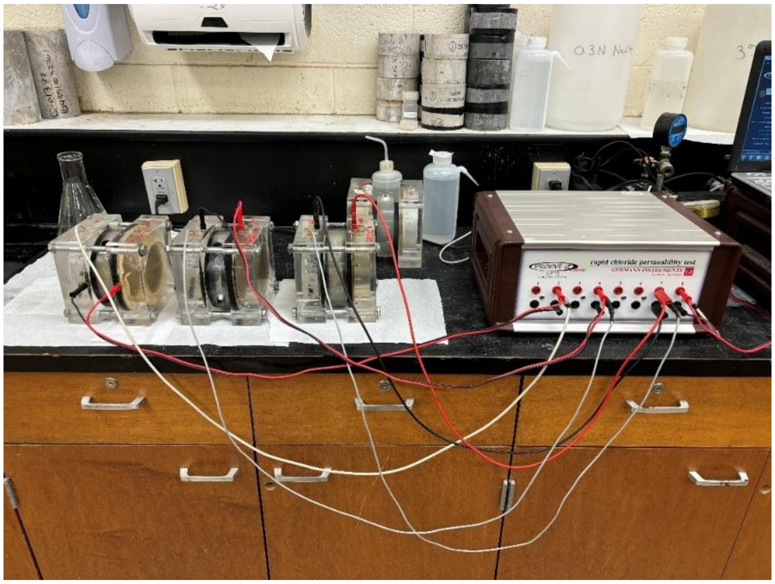

Figure 3.14 Rapid chloride permeability testing.

Figure 3.15 Sample drying for absorption measurements.

<u>3.3.5 Hardened Air Void Analyses</u>

Hardened air void analyses were performed on selected core samples in general accordance with ASTM C457 (Standard Practice for Microscopical Determination of Air Void Content and Parameters of Air Void System in Hardened Concrete) using Procedure B, which is the modified point-count method. The depth of analyses was limited to the upper approximately

2 in. of each core, where the analyses were performed on the two flat faces of a section of concrete that was cut from the center of each core, perpendicular to the wearing surface. A magnification of 108x was utilized for the analyses.

3.3.6 Chloride Concentration Analyses

For chloride concentration analyses, titration was performed in general accordance with ASTM C1152 (Standard Test Method for Acid-Soluble Chloride in Mortar and Concrete) on concrete powder samples collected during field research. The resulting chloride concentration was converted to units of pounds of chloride per cubic yard of concrete using the average unit weight of the concrete at each site as measured from the cores.

3.4 Summary

The scope of work included both field and laboratory research. For field research, six sites in northern Utah were selected by UDOT personnel for evaluation. At the time of inspection, the repairs had been in service for 4 to 5 years. At each site, three or four repairs were selected for evaluation. Visual inspection was used to prepare a distress map, or drawing, of each selected repair. Crack density, average crack width, and percent by area of scaling, spalling, delamination, and construction-related issues were computed. For Schmidt rebound hammer testing, resistivity testing, and concrete sampling, the specific location to be tested within each repair was marked following a predetermined procedure. Sampling involved concrete powder sampling and coring at each test location. Laboratory research, which was performed on samples removed from the test sites, included stiffness testing, compressive strength testing, splitting tensile strength testing, rapid chloride permeability testing, absorption measurements, hardened air void analyses, and chloride concentration analyses.

4.0 RESULTS

4.1 Overview

The scope of field and laboratory work performed for this research is summarized in Tables 4.1 and 4.2, respectively, and Appendix A provides supporting data. Repairs 2-3 and 4-1 were manually selected for evaluation in addition to the three randomly selected repairs at each site, leading to evaluation of a total of four repairs at sites 2 and 4. The results are expected to be applicable to rapid-setting concrete repairs with similar concrete mixture designs, construction practices, and service conditions to those studied in this research. The following sections provide a compilation and a discussion of the data.

Table 4.1 Field Research Summary

Site	Repair	Cover Depth Testing	Distress Surveys	Schmidt Rebound Hammer Testing	Resistivity Testing	Concrete Powder Sampling	Core Sampling
1	3		x	x	x	x	x
1	10		x	x	x	x	x
1	13		x	x	x	x	x
2	1		x	x	x	x	x
2	2		x	x	x	x	x
2	3		x	x	x	x	x
2	4		x	x	x	x	x
3	1	x	x	x	x	x	x
3	2	x	x	x	x	x	x
3	3	x	x	x	x	x	x
4	1	x	x	x	x	x	x
4	11	x	x	x	x	x	x
4	19	x	x	x	x	x	x
4	24	x	x	x	x	x	x
5	1		x	x	x	x	x
5	2		x	x	x	x	x
5	3		x	x	x	x	x
6	3		x	x	x	x	x
6	13		x	x	x	x	x
6	17		x	x	x	x	x

Table 4.2 Laboratory Research Summary

Site	Repair	Stiffness Testing	Compressive Strength Testing	Splitting Tensile Strength Testing	Rapid Chloride Permeability Testing	Absorption Measurements	Hardened Air Void Analyses	Chloride Concentration Analyses
1	3	x	x					x
1	10	x		x			x	x
1	13	x		x	x	x		x
2	1	x	x					x
2	2	x		x				x
2	3	x	x					x
2	4	x			x	x	x	x
3	1	x	x					x
3	2	x		x	x	x		x
3	3	x		x				x
4	1	x			x	x	x	x
4	11							x
4	19	x		x				x
4	24			x				x
5	1	x	x					x
5	2	x		x				x
5	3	x		x	x	x		x
6	3	x		x				x
6	13	x		x	x	x		x
6	17	x	x					x

4.2 Data Compilation

The results of the field and laboratory research were compiled for analysis as described in the following sections.

4.2.1 Field Research

The results of field research include distress maps and corresponding calculations, Schmidt rebound numbers, and resistivity values. Distress maps of the selected repairs at each site are shown in Appendix B, and corresponding photographs are shown in Appendix C. In the distress maps, cracks are shown in red, spalling is shown in magenta, delamination is shown in blue, and construction-related distresses are shown in orange; because of the high percentages of scaling at several sites, the drawings do not show that distress. The approximate location of the field testing is shown with a cyan marker that is drawn with dimensions of 1 ft by 1 ft, and the crack widths are labeled with the original measurement unit of millimeters. With respect to the position of the repair on the pavement panel or bridge deck, the approximate location of the wheel path is shown in gray, white lane markings are shown as black lines, and yellow lane markings are shown as yellow lines. In situations such as lane merges, wheel paths were not approximated. In all cases, the direction of traffic flow is from the bottom of the drawing or photograph to the top.

Based on the repair areas shown in Table 4.3, where applicable, distress data were compiled for analysis as shown in Tables 4.4 to 4.6. The results of Schmidt rebound hammer testing, including estimated concrete compressive strengths, are shown in Table 4.7. Resistivity data with corresponding surface temperatures are presented in Table 4.8. Regarding concrete sampling, photographs of the core samples are shown in Appendix D. Inspection of the cores indicated that the approximate nominal maximum aggregate size was 0.75 in. at sites 1, 2, 3, 5, and 6 and 0.375 in. at site 4. The aggregate for site 1 appeared to be particularly gap-graded, and the aggregate size at site 3, at which approach slab repairs were evaluated, was consistent with

Table 4.3 Repair Areas

Site	Repair	Area (ft^2)
1	3	72
1	10	87
1	13	86
2	1	74
2	2	109
2	3	113
2	4	207
3	1	85
3	2	37
3	3	16
4	1	12
4	11	79
4	19	32
4	24	38
5	1	93
5	2	92
5	3	48
6	3	62
6	13	112
6	17	55

Table 4.4 Crack Densities and Widths

Site	Repair	Crack Density (ft/ft^2)	Average Crack Width (mils)
1	3	0.419	33
1	10	0.158	36
1	13	0.072	49
2	1	0.000	0
2	2	0.022	12
2	3	0.072	33
2	4	0.008	24
3	1	0.403	26
3	2	0.560	26
3	3	0.098	13
4	1	1.435	17
4	11	0.818	14
4	19	0.629	23
4	24	0.678	18
5	1	0.096	394
5	2	0.166	198
5	3	0.166	399
6	3	0.030	132
6	13	0.009	33
6	17	0.005	24

requirements for pavement panels. At site 5, the appearance of the cores suggested that two different rapid-setting concrete mixtures may have been used at that site. Concrete cover depths, which were measured near test locations in evaluated repairs at the bridge deck and approach slab sites, ranged from 2.54 in. to 4.30 in. at site 3 and from 1.03 in. to 2.87 in. at site 4. Cover depth data are provided in Appendix A.

Table 4.5 Scaling, Spalling, and Delamination

Site	Repair	Scaling Area Density (%)	Spalling Area Density (%)	Delamination Area Density (%)
1	3	90.0	0.0	0.0
1	10	90.0	0.0	0.0
1	13	80.0	0.0	0.0
2	1	98.0	0.0	0.0
2	2	98.0	0.0	0.0
2	3	95.0	0.1	0.0
2	4	96.0	0.0	0.0
3	1	98.0	2.7	0.0
3	2	95.0	0.2	0.0
3	3	100.0	0.4	0.0
4	1	20.0	0.0	4.0
4	11	10.0	0.0	6.2
4	19	10.0	0.0	7.6
4	24	8.0	0.0	2.7
5	1	15.0	0.6	0.0
5	2	20.0	0.8	0.0
5	3	15.0	1.8	0.0
6	3	0.0	0.2	0.0
6	13	0.0	0.1	0.0
6	17	0.0	0.1	0.0

Table 4.6 Construction-Related Issues

Site	Repair	Construction Issues Area Density (%)
1	3	0.0
1	10	0.0
1	13	0.0
2	1	0.0
2	2	0.0
2	3	0.0
2	4	0.0
3	1	0.0
3	2	0.0
3	3	0.0
4	1	0.0
4	11	0.0
4	19	0.3
4	24	0.0
5	1	0.0
5	2	0.0
5	3	0.0
6	3	0.0
6	13	1.1
6	17	0.0

Table 4.7 Schmidt Rebound Numbers

Site	Repair	Schmidt Rebound Number				Estimated Compressive Strength (psi)
		Reading 1	Reading 2	Reading 3	Average	
1	3	40	42	42	41	5800
1	10	43	43	45	44	6300
1	13	45	47	53	48	7400
2	1	46	47	48	47	7100
2	2	44	45	47	45	6700
2	3	25	29	29	28	3100
2	4	45	46	46	46	6800
3	1	51	52	58	54	8500
3	2	52	54	56	54	8600
3	3	54	55	55	55	8700
4	1	36	38	40	38	5100
4	11	49	50	51	50	7700
4	19	46	51	54	50	7800
4	24	45	46	52	48	7200
5	1	40	40	40	40	5500
5	2	40	41	41	41	5700
5	3	45	45	46	45	6700
6	3	49	51	52	51	7900
6	13	52	54	55	54	8500
6	17	51	52	54	52	8200

Table 4.8 Resistivity Values

Site	Repair	Resistivity (kohm-in.)			Surface Temperature (°F)
		Location 1	Location 2	Average	
1	3	39.9	40.1	40.0	91
1	10	40.3	37.8	39.0	92
1	13	40.8	40.4	40.6	92
2	1	40.5	39.9	40.2	92
2	2	40.8	40.8	40.8	92
2	3	40.6	40.6	40.6	90
2	4	41.0	40.8	40.9	92
3	1	40.2	40.1	40.2	79
3	2	40.4	39.9	40.2	81
3	3	40.4	40.1	40.2	80
4	1	40.3	40.4	40.4	90
4	11	40.2	40.2	40.2	89
4	19	40.6	40.6	40.6	89
4	24	40.6	40.6	40.6	87
5	1	38.0	37.3	37.6	72
5	2	35.5	35.7	35.6	71
5	3	32.0	37.7	34.9	70
6	3	39.6	36.8	38.2	73
6	13	35.2	38.2	36.7	72
6	17	38.6	37.5	38.1	72

4.2.2 Laboratory Research

The results of laboratory research include stiffness, compressive strength, splitting tensile strength, rapid chloride permeability, and absorption values, as well as hardened air void analyses and chloride concentration analyses. Compressive strength testing was not performed on cores from site 4 because the cores were too short to be tested. Hardened air void analyses were performed on three cores that were selected to provide results for rapid-setting concrete repairs comprising different mixture designs and a repair that exhibited a noticeably lower unit weight; all three cores exhibited scaling.

The data are presented in Tables 4.9 to 4.14. In a few of these tables, two cores, 4-1-1 and 4-1-2, are shown for repair 1 at site 4; the second core was removed when the first core was observed to be short. Regarding stiffness testing, the short lengths of cores 4-1-1 and 4-1-2,

Table 4.9 Stiffness Values

Site	Repair	Unit Weight (pcf)	Young's Modulus (ksi)
1	3	139.6	5201
1	10	138.7	5235
1	13	137.8	4845
2	1	134.2	5234
2	2	135.8	5431
2	3	133.1	4739
2	4	132.5	4537
3	1	133.7	4813
3	2	137.7	5183
3	3	136.5	5396
4	1-1	122.1	2204
4	1-2	121.1	3465
4	19	123.9	3647
5	1	137.4	5124
5	2	134.2	4497
5	3	134.9	4968
6	3	135.6	5005
6	13	134.4	5070
6	17	136.9	5160

Table 4.10 Compressive Strengths

Site	Repair	Unit Weight (pcf)	Compressive Strength (psi)
1	3	139.6	9365
2	1	134.2	9327
2	3	133.1	5213
3	1	133.7	10867
5	1	137.4	8493
6	17	136.9	10496

Table 4.11 Splitting Tensile Strengths

Site	Repair	Unit Weight (pcf)	Splitting Tensile Strength (psi)
1	10	135.8	705
1	13	136.5	792
2	2	133.1	780
2	2	133.3	711
3	2	136.5	862
3	3	135.5	669
4	19	122.9	801
4	24	122.9	840
5	2	132.1	642
5	2	130.8	671
5	3	132.3	857
6	3	133.2	864
6	3	132.6	826
6	13	132.6	838

Table 4.12 Rapid Chloride Permeability and Absorption Values

Site	Repair	Unit Weight (pcf)		Chloride Permeability	Absorption
		Soaked	Dry	(C)	(%)
1	13	137.1	124.7	545	9.9
2	4	133.9	123.6	81	8.3
3	2	135.9	126.4	126	7.5
4	1-1	123.5	113.5	140	8.8
5	3	136.1	125.0	272	8.9
6	13	132.8	123.6	89	7.5

Table 4.13 Hardened Air Void Values

Property	Core Sample		
	1-10	2-4	4-1-2
Unit Weight (pcf)	137.1	131.1	120.1
Total Air Void Content (%)	4.6	7.2	11.9
Voids Larger Than 1 mm (%)	1.0	0.6	3.7
Specific Surface (in.^{2}/in.^{3})	700	947	469
Spacing Factor (in.)	0.0080	0.0049	0.0057
Void Frequency (voids/in.)	8.1	16.9	13.9
Cement Paste Content (%)	34.8	35.6	31.8
Paste-Air Ratio	7.6	5.0	2.7
Traverse Length (in.^{2})	93.4	80.5	76.3
Traverse Area (in.^{2})	17.6	17.6	18.4
Number of Stops	1868	1609	1526

Table 4.14 Chloride Concentrations

Site	Repair	Average Unit Weight (pcf)	Chloride Concentration (lb Cl^- / yd^3 concrete)			
			0-1 in.	1-2 in.	2-3 in.	3-4 in.
1	3	138.7	8.9	2.4	0.8	0.6
1	10		9.8	2.1	0.7	0.6
1	13		8.0	1.1	0.8	0.7
2	1	133.9	2.1	0.7	0.2	0.1
2	2		3.5	0.8	<0.1	<0.1
2	3		4.8	4.3	0.6	0.5
2	4		3.3	0.6	0.3	0.2
3	1	136.0	5.5	1.3	0.5	0.4
3	2		2.2	1.1	0.8	0.6
3	3		5.7	1.3	0.8	1.0
4	1	122.7	5.0	1.1	1.4	2.7
4	11		5.2	2.0	3.8	4.3
4	19		4.1	0.7	1.0	3.8
4	24		5.0	1.5	2.0	3.6
5	1	135.5	12.2	3.0	1.4	1.3
5	2		12.8	2.8	1.1	1.3
5	3		9.6	2.1	1.1	1.0
6	3	135.6	1.5	0.7	0.5	0.6
6	13		1.4	0.5	0.4	0.5
6	17		1.4	0.5	0.5	0.5

which were 2.8 in. and 2.4 in., respectively, may have yielded artificially low modulus of elasticity values. For compressive strength testing of core 5-1, the compression machine automatically stopped the test when one of the edges of the core initially broke. Because the load was smaller than expected based on the results obtained for the other specimens, the core was tested again without the piece that had previously broken, and it sustained a higher load, which is reflected in Table 4.10. Also, because the ratio of the length to the diameter for core 2-3 was 2.17, which is just greater than the maximum value of 2.1 recommended in ASTM C42, the resulting compressive strength, which was the lowest value measured, is considered to be conservative. Regarding splitting tensile strength testing, the full lengths of cores 3-3, 4-19, and 4-24 were evaluated, the upper portions of cores 1-13, 3-2, 5-3, and 6-13 were evaluated, the lower portion of core 1-10 was evaluated, and the top and bottom portions of cores 2-2, 5-2, and 6-3 were evaluated. Regarding hardened air void analyses, the top portions of cores 1-10 and 2-4 and the full length of core 4-1-2 were selected for evaluation because cores 1-10 and 2-4 had a larger nominal maximum aggregate size of 0.75 in., core 1-10 was batched with different coarse aggregate than cores 2-4 and 4-1-2, and core 4-1-2 had a smaller nominal maximum aggregate size of 0.375 in. and a lower unit weight; in the results, air voids are displayed with the original measurement unit of millimeters for one parameter, and microscope photographs from hardened air void analyses are shown in Appendix E. Regarding chloride concentration testing, at cover depths of approximately 3 to 4 in. and 1 to 3 in. that were measured at sites 3 and 4, respectively, the corresponding ranges in chloride concentration were 0.4 to 1.0 lb Cl^-/yd^3 of concrete and 0.7 to 3.8 lb Cl^-/yd^3 of concrete.

4.3 Discussion

The field and laboratory research results are discussed in the following sections.

4.3.1 Field Research

The areas of evaluated repairs ranged from 12 to 207 ft^2, as shown in Table 4.3, with the average evaluated repair area being 75 ft^2. Cracking was observed at all six sites, scaling was observed at five sites, spalling was observed at four sites, delamination was observed at one site, and construction-related issues were observed at two sites. Cracking and scaling were therefore observed to be the most prevalent distresses among the sites evaluated in this research. In particular, given that delamination is often caused by corrosion of reinforcing steel at sites in cold regions, this distress was not prevalent because the majority of the sites were pavement panels rather than approach slabs or bridge decks, for example, as shown in Table 3.1.

For repair areas where these distresses were observed, crack densities ranged from 0.005 ft/ft^2 to 0.818 ft/ft^2, excluding the highest crack density of 1.435 ft/ft^2 that was observed at repair 4-1, which was manually selected and therefore not necessarily representative of the site, and average crack widths ranged from 12 to 399 mils. The percentage of surface area affected by scaling ranged from 8.0 to 100.0 percent, and the percentage of surface area that exhibited spalling ranged from 0.1 to 2.7 percent. The percentage of surface area that was characterized by delamination, which was observed at only the bridge deck site, ranged from 2.7 to 7.6 percent. Finally, the percentage of surface area that was affected by construction-related issues, including a surface gouge and a misshaped edge, ranged from 0.3 to 1.1 percent. Among these distresses, cracking and scaling were therefore observed to be the most extensive when present within a repair area.

Average Schmidt rebound numbers for the repairs evaluated in this research ranged from 40 to 55, which corresponds to a range of 5500 to 8700 psi; this range excludes the lowest average Schmidt rebound numbers of 28 and 38, corresponding to 3100 and 5100 psi, that were observed at repairs 2-3 and 4-1, respectively, which were manually selected and therefore not necessarily representative of the site. Average resistivity values ranged from 34.9 to 40.9 kohm-in., which all correspond to a corrosion potential classification of “low” (Barrus, 2012) and therefore indicate that steel embedded in the concrete would have a low probability of corrosion.

Regarding the manually selected repairs, repairs 2-3 and 4-1 exhibited a noticeably higher severity of material-related distress than the other repairs at the respective sites. In general, repair 2-3 exhibited a lower average Schmidt rebound number and higher crack density and average crack width relative to the other repairs at site 2, and repair 4-1 exhibited a lower average Schmidt rebound number and higher crack density and scaling relative to the other repairs at site 4. Thus, repairs that were manually selected were observed to exhibit lower average Schmidt rebound numbers and higher crack density, average crack width, and scaling than other repairs at the same sites.

Regarding the effects of traffic loading, the test locations for repairs 2-1, 2-2, 3-3, 5-1, and 6-3, which were all randomly selected, were positioned at least partially in a wheel path as shown in the corresponding distress maps in Appendix B. In general, while test locations 2-1, 2-2, and 3-3 did not exhibit notable differences relative to the other test locations at sites 2 and 3, test locations 5-1 and 6-3 exhibited a slightly lower average Schmidt rebound number relative to the other test locations at sites 5 and 6. Thus, test locations positioned at least partially in a wheel path were observed to exhibit no notable differences or to exhibit slightly lower average Schmidt rebound numbers than other test locations at the same sites.

4.3.2 Laboratory Research

Regarding cores removed from the randomly selected repairs, stiffness ranged from 3647 to 5431 ksi, and compressive strength ranged from 8493 to 10867 psi. All compressive strengths, including the lowest value of 5213 psi measured for core 2-3, exceeded the minimum compressive strength of 5200 psi required by UDOT for rapid strength concrete (UDOT, 2024c). Splitting tensile strength ranged from 642 to 864 psi. RCPT values ranged from 81 to 545 C, corresponding to classifications of “negligible” or “very low” chloride permeability, and the absorption values of these specimens ranged from 7.5 to 9.9 percent.

The hardened air void analyses indicated total air contents ranging from 4.6 to 11.9 percent for the evaluated cores. Core 4-1-2, which was the only core removed from a manually selected repair that was selected for hardened air void analyses, exhibited the highest total air void content of 11.9 percent, which is above the upper limit of 7.5 percent specified by UDOT, while core 1-10 exhibited the lowest total air void content of 4.6 percent, which is below the lower limit of 5.0 percent specified by UDOT. The analyses also showed a cement paste content of 31.8 to 35.6 percent and a paste-air ratio of 2.7 to 7.6. Microscope photographs provided in Appendix E show a generally lighter color of cement paste in the upper portions of the analyzed core depths, which indicates a lower amount of cementitious products typical of a higher water-cement ratio, possibly caused by improper finishing practices; shallow crazing cracks were also observed through the depth of the lighter color of cement paste, suggesting inadequate surface curing for those repairs.

The chloride concentration analyses showed that, in general, chloride concentration decreases with increasing depth; site 4 was an exception, where the testing apparently extended below the partial-depth patches and into the original underlying concrete, which had higher chloride concentrations. Overall, chloride concentrations ranged from less than 0.1 to 12.8 lb Cl^-/yd^3 of concrete within the upper 4 in. of the tested pavement panel or bridge deck, with the highest chloride concentrations being observed at site 5; because site 5 is located in a more mountainous region, it may have been exposed to more deicing salts. Regarding repairs at which reinforcing steel was present, the chloride concentration threshold of 2.0 lb Cl^-/yd^3 of concrete at which corrosion of reinforcing steel begins was exceeded at site 4 at the depth of the steel, which was likely below the shallow rapid-setting concrete repair.

Regarding the manually selected repairs, repair 2-3 exhibited lower compressive strength and higher chloride concentrations relative to the other repairs at site 2, and repair 4-1 exhibited lower stiffness relative to the other repairs at site 4. Thus, although the comparisons are limited because not all repairs were subjected to all laboratory tests, repairs that were manually selected were observed to exhibit lower stiffness and compressive strength and higher chloride concentrations than other repairs at the same sites.

Regarding the effects of traffic loading at test locations that were positioned at least partially in a wheel path, test locations 2-1 and 2-2 exhibited higher stiffness relative to the other randomly selected test location at site 2, test location 3-3 exhibited a lower splitting tensile strength and slightly higher stiffness and chloride concentrations relative to other test locations at site 3, test location 5-1 exhibited slightly higher stiffness relative to other test locations at site 5, and test location 6-3 did not exhibit notable differences relative to other test locations at site 6. Thus, test locations positioned at least partially in a wheel path were observed to exhibit no notable differences or to exhibit unexpectedly higher stiffness, lower splitting tensile strength, and slightly higher chloride concentrations than other test locations at the same sites.

4.4 Summary

The results are expected to be applicable to rapid-setting concrete repairs with similar concrete mixture designs, construction practices, and service conditions as those studied in this research. In summary, the results of field research include distress maps and corresponding calculations, Schmidt rebound numbers, and resistivity values. Cracking and scaling were observed to be the most prevalent distresses among the sites evaluated in this research.

Excluding manually selected repairs, Schmidt rebound numbers ranged from 40 to 55, which corresponds to a range of 5500 to 8700 psi, and all resistivity values correspond to a corrosion potential classification of "low."

The results of laboratory research include stiffness, compressive strength, splitting tensile strength, rapid chloride permeability, and absorption values, as well as hardened air void analyses and chloride concentration analyses. Stiffness values ranged from 3647 to 5431 ksi. All compressive strength values, which ranged from 5213 to 10867 psi, exceeded the minimum compressive strength of 5200 psi required by UDOT. Splitting tensile strength values ranged from 642 to 864 psi. RCPT values corresponded to classifications of "negligible" or "very low" chloride permeability, and the absorption values of these specimens ranged from 7.5 to 9.9 percent. The hardened air void analyses indicated total air contents ranging from 4.6 to 11.9 percent, where the lowest and highest total air contents are outside the limits specified by UDOT. Microscope photographs suggest improper finishing practices and inadequate surface curing for those cores.

The chloride concentration analyses showed that, in general, chloride concentration decreases with increasing depth, and, overall, chloride concentrations ranged from less than 0.1 to 12.8 lb Cl^-/yd^3 of concrete within the upper 4 in. of the tested pavement panel or bridge deck. Regarding repairs at which reinforcing steel was present, the chloride concentration threshold of 2.0 lb Cl^-/yd^3 of concrete at which corrosion of reinforcing steel begins was exceeded at site 4 at the depth of the steel, which was likely below the shallow rapid-setting concrete repair.

In field testing, repairs that were manually selected because they exhibited a noticeably higher severity of material-related distress than the other repairs at the respective sites were observed to exhibit lower average Schmidt rebound numbers and higher crack density, average crack width, and scaling than other repairs at the same sites. In laboratory testing, although the comparisons are limited because not all repairs were subjected to all laboratory tests, repairs that were manually selected were observed to exhibit lower stiffness and compressive strength and higher chloride concentrations than other repairs at the same sites.

Regarding the effects of traffic loading, test locations positioned at least partially in a wheel path were observed to exhibit no notable differences or to exhibit slightly lower average Schmidt rebound numbers than other test locations at the same sites. In laboratory testing, test locations positioned at least partially in a wheel path were observed to exhibit no notable differences or to exhibit unexpectedly higher stiffness, lower splitting tensile strength, and slightly higher chloride concentrations than other test locations at the same sites.

5.0 CONCLUSION

5.1 Summary

The objective of this research was to evaluate the durability of rapid-setting concrete batched using volumetric concrete mixers and placed in a cold region. The scope of work included field and laboratory evaluations of rapid-setting concrete repairs on both pavement panels and bridge decks in Utah. For field research, six sites in northern Utah were selected by UDOT personnel for evaluation. At the time of inspection, the repairs had been in service for 4 to 5 years. At each site, three or four repairs were selected for evaluation. Visual inspection was used to prepare a distress map, or drawing, of each selected repair. Crack density, average crack width, and percent by area of scaling, spalling, delamination, and construction-related issues were computed. For Schmidt rebound hammer testing, resistivity testing, and concrete sampling, the specific location to be tested within each repair was marked following a predetermined procedure. Sampling involved concrete powder sampling and coring at each test location. Laboratory research, which was performed on samples removed from the test sites, included stiffness testing, compressive strength testing, splitting tensile strength testing, rapid chloride permeability testing, absorption measurements, hardened air void analyses, and chloride concentration analyses.

5.2 Findings

The results are expected to be applicable to rapid-setting concrete repairs with similar concrete mixture designs, construction practices, and service conditions as those studied in this research. In summary, the results of field research include distress maps and corresponding calculations, Schmidt rebound numbers, and resistivity values. Cracking and scaling were observed to be the most prevalent distresses among the sites evaluated in this research. Excluding manually selected repairs, Schmidt rebound numbers ranged from 40 to 55, which corresponds to a range of 5500 to 8700 psi, and all resistivity values correspond to a corrosion potential classification of “low.”

The results of laboratory research include stiffness, compressive strength, splitting tensile strength, rapid chloride permeability, and absorption values, as well as hardened air void analyses and chloride concentration analyses. Stiffness values ranged from 3647 to 5431 ksi. All compressive strength values, which ranged from 5213 to 10867 psi, exceeded the minimum compressive strength of 5200 psi required by UDOT. Splitting tensile strength values ranged from 642 to 864 psi. RCPT values corresponded to classifications of "negligible" or "very low" chloride permeability, and the absorption values of these specimens ranged from 7.5 to 9.9 percent. The hardened air void analyses indicated total air contents ranging from 4.6 to 11.9 percent, where the lowest and highest total air contents are outside the limits specified by UDOT. Microscope photographs suggest improper finishing practices and inadequate surface curing for those cores.

The chloride concentration analyses showed that, in general, chloride concentration decreases with increasing depth, and, overall, chloride concentrations ranged from less than 0.1 to 12.8 lb Cl^-/yd^3 of concrete within the upper 4 in. of the tested pavement panel or bridge deck. Regarding repairs at which reinforcing steel was present, the chloride concentration threshold of 2.0 lb Cl^-/yd^3 of concrete at which corrosion of reinforcing steel begins was exceeded at site 4 at the depth of the steel, which was likely below the shallow rapid-setting concrete repair.

In field testing, repairs that were manually selected because they exhibited a noticeably higher severity of material-related distress than the other repairs at the respective sites were observed to exhibit lower average Schmidt rebound numbers and higher crack density, average crack width, and scaling than other repairs at the same sites. In laboratory testing, although the comparisons are limited because not all repairs were subjected to all laboratory tests, repairs that were manually selected were observed to exhibit lower stiffness and compressive strength and higher chloride concentrations than other repairs at the same sites.

Regarding the effects of traffic loading, test locations positioned at least partially in a wheel path were observed to exhibit no notable differences or to exhibit slightly lower average Schmidt rebound numbers than other test locations at the same sites. In laboratory testing, test locations positioned at least partially in a wheel path were observed to exhibit no notable differences or to exhibit unexpectedly higher stiffness, lower splitting tensile strength, and slightly higher chloride concentrations than other test locations at the same sites.

5.3 Recommendations

Several recommendations based on the results of this research and information obtained from the literature were developed. Regarding mixture design of rapid-setting concrete, use of excessive cement, which can be manifest as high stiffness, compressive strength, and splitting tensile strength, should be avoided to minimize cracking; high cement contents can lead to cracking as a result of brittleness of the hardened concrete. Furthermore, use of appropriate amounts of air-entraining admixtures is recommended to ensure adequate resistance to freeze-thaw damage in cold regions; testing should be performed to ensure that rapid-setting concrete repairs placed in Utah have an air content between 5.0 and 7.5 percent, consistent with UDOT specifications. Regarding construction, rapid-setting concrete must be properly finished and cured to provide a durable surface that is resistant to scaling. Accomplishing the required testing and providing sufficient time for proper finishing can be accomplished using set-retarding admixtures. Pre-wetting prepared repair areas using chilled water is also recommended before placement of rapid-setting concrete repairs. Curing practices may involve application of PAMS or pre-soaked burlap, for example. With additional emphasis on these points, facilitated through contractor training and/or rapid-setting concrete manufacturer representation on site, as necessary, rapid-setting concrete batched using volumetric concrete mixers should continue to be used for repairs of concrete pavement panels and bridge decks in Utah to expedite the concrete curing process and thereby minimize the impacts of lane closures on traffic.

REFERENCES

Barrus, N. C. 2012. *Sensitivity of resistivity measurements on concrete bridge decks to operator-controlled and concrete material variables*. M.S. thesis. Provo, UT: Brigham Young University. https:notio//scholarsarchive.byu.edu/etd/3203/.

Cemmac. 2018. "Universal 32,5 R." Accessed March 28, 2025. http://www.cemmac.sk/dev/language/en/universal-325-r-2/.

CTS Cement Manufacturing Corporation. 2023. "Rapid set cement: Rapid hardening hydraulic cement." *CTS Cement*. Accessed December 17, 2024. https://www.ctscement.com/datasheet/RAPID_SET_CEMENT_Datasheet_DS_012_EN?c=&t=Professionals.

CTS Cement Manufacturing Corporation. 2025. "Concrete mix: Very rapid hardening concrete." *CTS Cement*. Accessed April 17, 2025. https://www.ctscement.com/datasheet/CONCRETE_MIX_Datasheet_DS_004_EN.

de Bruyn, K., E. Bescher, C. Ramseyer, S. Hong, and T. H. Kang. 2017. "Pore structure of calcium sulfoaluminate paste and durability of concrete in freeze-thaw environment." *International Journal of Concrete Structures and Materials*, 11 (1), 59–68. https://doi.org/10.1007/s40069-016-0174-3.

Edwards, L., W. D. Carruth, J. S. Tingle, and I. L. Howard. 2018. *Rapid-setting flowable fill performance in cold weather for airfield damage repair*. ERDC/GSL TR-18-26. U.S. Army Engineer Research and Development Center, Vicksburg, MS.

Guo, X., H. Shi, W. Hu, and K. Wu. 2014. "Durability and microstructure of CSA cement-based materials from MSWI fly ash." *Cement and Concrete Composites*, 46, 26–31. https://doi.org/10.1016/j.cemconcomp.2013.10.015.

Guthrie, W. S., L. H. Yuen, and L. A. Ross. 2005. *Performance of concrete bridge deck joints*. Report UT-05.04. Utah Department of Transportation, Salt Lake City, UT.

Hendricks, L., J. S. Baxter, Y. Chou, M. Thomas, E. Boekweg, W. S. Guthrie, and B. A. Mazzeo. 2020. “High-speed acoustic impact-echo sounding of concrete bridge decks.” *Journal of Nondestructive Evaluation*, 39 (58), 1–12. https://doi.org/10.1007/s10921-020-00695-0.

Huang, Y. H. 2004. *Pavement analysis and design*. 2nd ed. Pearson Education, Upper Saddle River, NJ.

Jewell, R. B., R. F. Rathbone, T. Y. Duvallet, T. L. Robl, and K. C. Mahboub. 2015. “Fabrication and testing of low-energy calcium sulfoaluminate-belite cements that utilize circulating fluidized bed combustion by-products.” *Coal Combustion and Gasification Products*, 7, 9-18. https://doi.org/10.4177/CCGP-D-15-00001.1.

Mallela, J., and S. Sadasivam. 2011. *Work zone road user costs: Concepts and applications*. FHWA-HOP-12-005. U. S. Department of Transportation, Washington, DC.

Miller, J. S., and W. Y. Bellinger. 2003. *Distress identification manual for the long-term pavement performance program.* 4th ed. Publication FHWA-RD-03-031. Federal Highway Administration, McLean, VA.

Mindess, S., J. F. Young, and D. Darwin. 2003. *Concrete*. 2nd ed. Pearson Education, Upper Saddle River, NJ.

Moffatt, E. G. 2016. *Durability of rapid-set (ettringite-based) concrete*. Ph.D. dissertation. Fredericton, New Brunswick, Canada: University of New Brunswick.

Moffatt, E. G., and M. D. A. Thomas. 2018. "Durability of rapid-strength concrete produced with ettringite-based binders." *ACI Materials Journal*, 115 (1), 105–115. https://doi.org/10.14359/51701006.

Priddy, L. P., H. P. Bell, L. Edwards, W. D. Carruth, and J. F. Rowland. 2016. *Evaluation of the structural performance of CTS rapid set concrete mix*. ERDC/GSL TR-16-20. Army Engineer Research and Development Center, Vicksburg, MS.

Stevens, R. J., W. S. Guthrie, J. S. Baxter, and B. A. Mazzeo. 2021. "Field evaluation of polyester-polymer concrete overlays on bridge decks using nondestructive testing." J. Mater. Civ. Eng., 33 (7): 04021155. https://doi.org/10.1061/(ASCE)MT.1943-5533.0003810.

UDOT (Utah Department of Transportation). 2024a. "Portland cement concrete pavement, Section 02752." *Standard specifications for road and bridge construction*, Utah Department of Transportation, Salt Lake City, UT.

UDOT. 2024b. "Portland cement concrete, Section 03055." *Standard specifications for road and bridge construction*, UDOT, Salt Lake City, UT.

UDOT. 2024c. "Rapid strength concrete, Section 03058." *Standard specifications for road and bridge construction*, UDOT, Salt Lake City.

UDOT. 2024d. "Concrete curing, Section 03390." *Standard specifications for road and bridge construction*. UDOT, Salt Lake City, UT.

Zhang, G., Y. Yang, H. Yang, and H. Li. 2020. "Calcium sulphoaluminate cement used as mineral accelerator to improve the property of Portland cement at sub-zero temperature." *Cement and Concrete Composites*, 106, 1–12. https://doi.org/10.1016/j.cemconcomp.2019.103452.

Zhao, J., G. Cai, D. Gao, and S. Zhao. 2014. “Influences of freeze-thaw cycle and curing time on chloride ion penetration resistance of sulphoaluminate cement concrete.” *Const. and Build. Mat.,* 53, 305–311. https://doi.org/10.1016/j.conbuildmat.2013.11.110.

APPENDIX A: SUPPORTING DATA

In Figures A.1 to A.7, black lines represent reinforcing steel, and measured cover depths are shown in units of inches. In all cases, the direction of traffic is from the bottom of the figure to the top.

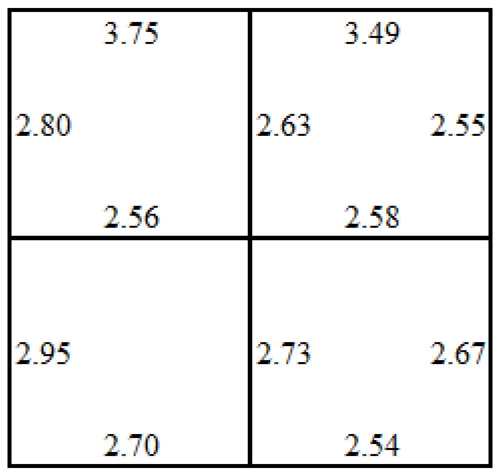

Figure A.1 Cover depths for repair 3-1.

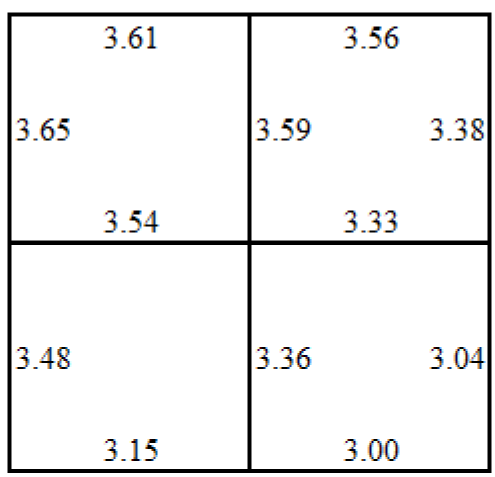

Figure A.2 Cover depths for repair 3-2.

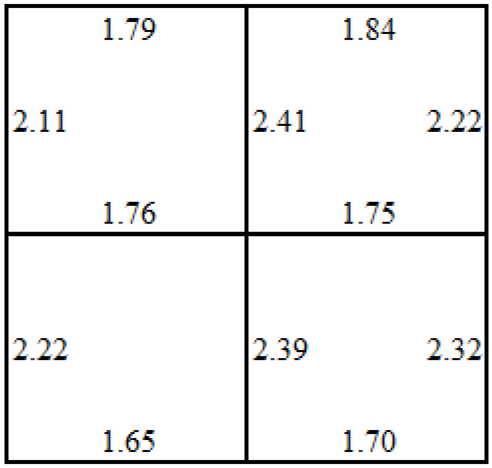

Figure A.3 Cover depths for repair 3-3.

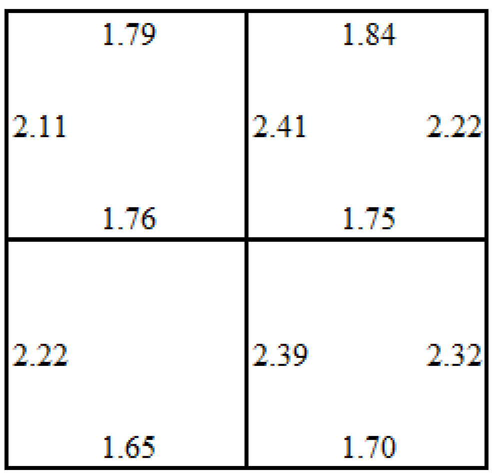

Figure A.4 Cover depths for repair 4-1.

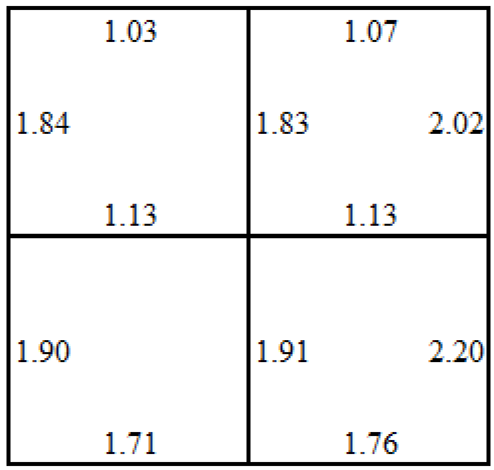

Figure A.5 Cover depths for repair 4-11.

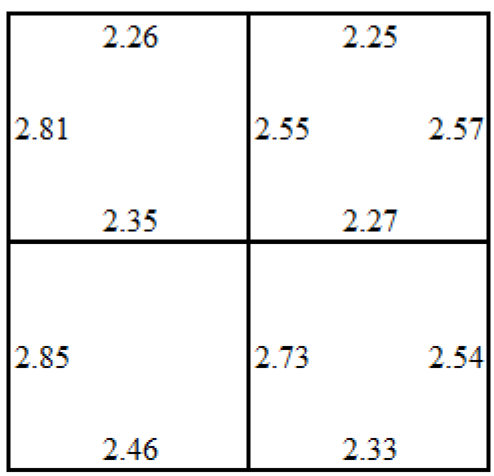

Figure A.6 Cover depths for repair 4-19.

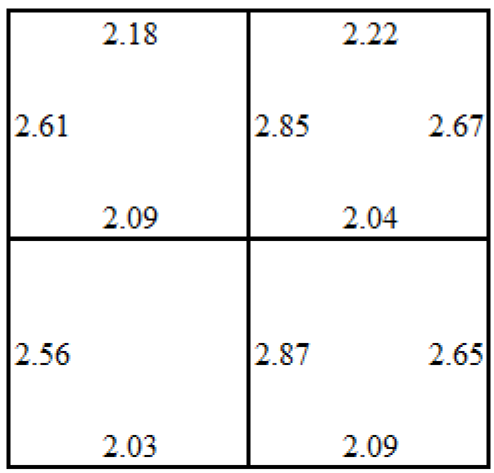

Figure A.7 Cover depths for repair 4-24.

Table A.1 Crack Density Data

Site	Repair	Area (ft^2)	Total Length of Cracks (ft)
1	3	72	30.1
1	10	87	13.8
1	13	86	6.2
2	1	74	0.0
2	2	109	2.4
2	3	113	8.0
2	4	207	1.7
3	1	85	34.3
3	2	37	20.8
3	3	16	1.6
4	1	12	16.9
4	11	79	64.6
4	19	32	20.1
4	24	38	26.1
5	1	93	8.9
5	2	92	15.2
5	3	48	8.0
6	3	62	1.8
6	13	112	1.1
6	17	55	0.3

Table A.2 Resistivity Data

Site	Repair	Resistivity (kohm-in.)				Surface Temperature (°F)
		Location 1		Location 2		
		Reading 1	Reading 2	Reading 1	Reading 2	
1	3	40.6	39.2	40.0	40.1	91
1	10	40.3	40.3	37.8	37.8	92
1	13	40.9	40.7	40.3	40.4	92
2	1	40.4	40.6	40.0	39.9	92
2	2	40.9	40.7	40.8	40.7	92
2	3	40.7	40.6	40.6	40.6	90
2	4	41.0	41.0	40.8	40.9	92
3	1	40.2	40.2	40.1	40.2	79
3	2	40.4	40.4	40.0	39.9	81
3	3	40.4	40.4	40.1	40.1	80
4	1	40.2	40.4	40.1	40.6	90
4	11	40.2	40.2	40.0	40.5	89
4	19	40.7	40.5	40.6	40.6	89
4	24	40.6	40.6	40.6	40.6	87
5	1	38.0	38.0	37.3	37.3	72
5	2	35.6	35.4	35.7	35.7	71
5	3	32.3	31.8	37.7	37.6	70
6	3	39.7	39.6	36.9	36.7	73
6	13	35.2	35.2	38.2	38.1	72
6	17	38.7	38.6	37.5	37.4	72

Table A.3 Stiffness Data

Site	Repair	Unit Weight (pcf)	Length (ft)	Resonant Frequency (Hz)	Young's Modulus (psi)
1	3	139.6	0.6671	9852.0	5201105
1	10	138.7	0.6664	9924.3	5234744
1	13	137.8	0.5760	11084.4	4844702
2	1	134.2	0.6796	9892.8	5233998
2	2	135.8	0.6894	9877.2	5431101
2	3	133.1	0.7288	8815.5	4738739
2	4	132.5	0.3559	17696.8	4536606
3	1	133.7	0.4991	12943.8	4812829
3	2	137.7	0.3185	20736.9	5182587
3	3	136.5	0.3958	17102.0	5396192
4	1-1	122.1	0.2323	19696.8	2204486
4	1-2	121.1	0.1995	28863.9	3464588
4	19	123.9	0.2716	21512.7	3646672
5	1	137.4	0.6506	10105.4	5124072
5	2	134.2	0.6314	9872.3	4497459
5	3	134.9	0.5647	11569.0	4967933
6	3	135.6	0.6441	10153.9	5005379
6	13	134.4	0.5413	12215.9	5069849
6	17	136.9	0.6898	9584.5	5160369

Table A.4 Compressive Strength Data

Site	Repair	Length (in.)	Diameter (in.)	Ratio of Length to Diameter	Correction Factor	Load (lb)	Compressive Strength (psi)
1	3	8.0050	4.0271	1.99		119285	9365
2	1	8.1558	3.9983	2.04		117115	9327
2	3	8.7459	4.0263	2.17		66375	5213
3	1	5.9894	4.0270	1.49	0.96	144405	10867
5	1	7.8078	4.0206	1.94		107830	8493
6	17	8.2775	4.0146	2.06		132865	10496

Table A.5 Splitting Tensile Strength Data

Site	Repair	Unit Weight (pcf)	Length (in.)	Diameter (in.)	Applied Compressive Load (lb)	Splitting Tensile Strength (psi)
1	10	135.8	3.8420	4.0153	17095	705
1	13	136.5	4.7960	4.0220	24010	792
2	2	133.1	4.1745	4.0135	20530	780
2	2	133.3	4.0283	4.0260	18125	711
3	2	136.5	1.7350	4.0250	9460	862
3	3	135.5	4.7525	4.0073	20020	669
4	19	122.9	3.2518	4.0283	16480	801
4	24	122.9	2.1065	4.0280	11195	840
5	2	132.1	3.7963	4.0268	15415	642
5	2	130.8	3.6735	4.0298	15605	671
5	3	132.3	4.6060	4.0258	24975	857
6	3	133.2	3.8298	4.0245	20915	864
6	3	132.6	3.7538	4.0195	19580	826
6	13	132.6	4.3805	4.0248	23200	838

Table A.6 Rapid Chloride Permeability and Absorption Data

Site	Repair	Weight (lb)		Length (in.)	Diameter (in.)
		Soaked	Dry		
1	13	2.02	1.8375	1.9951	4.0315
2	4	1.943	1.7935	1.9670	4.0293
3	2	2.006	1.8665	1.9993	4.0305
4	1-1	1.8815	1.7295	2.0610	4.0335
5	3	2.034	1.8685	2.0176	4.0370
6	13	1.95	1.8145	1.9819	4.0373

Table A.7 Chloride Concentration Data

Site	Repair	Chloride Concentration (Percent by Weight)			
		0-1 in.	1-2 in.	2-3 in.	3-4 in.
1	3	0.238	0.065	0.022	0.015
1	10	0.262	0.055	0.019	0.017
1	13	0.214	0.030	0.022	0.020
2	1	0.058	0.019	0.005	0.004
2	2	0.097	0.022	BDL	BDL
2	3	0.134	0.120	0.017	0.015
2	4	0.090	0.017	0.009	0.006
3	1	0.151	0.035	0.013	0.012
3	2	0.061	0.031	0.023	0.015
3	3	0.155	0.035	0.021	0.028
4	1	0.151	0.034	0.043	0.081
4	11	0.157	0.061	0.114	0.130
4	19	0.125	0.023	0.030	0.115
4	24	0.152	0.045	0.061	0.108
5	1	0.334	0.081	0.039	0.034
5	2	0.350	0.076	0.030	0.036
5	3	0.262	0.059	0.030	0.026
6	3	0.041	0.020	0.014	0.016
6	13	0.039	0.013	0.012	0.013
6	17	0.039	0.014	0.014	0.013

APPENDIX B: DISTRESS MAPS

In the distress surveys, crack widths are labeled in mm (1 mm = 39.4 mils).

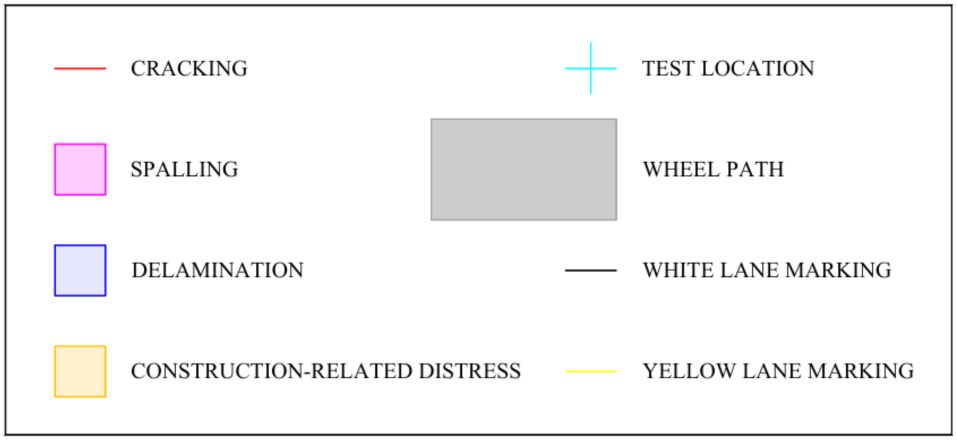

Figure B.1 Legend for distress maps.

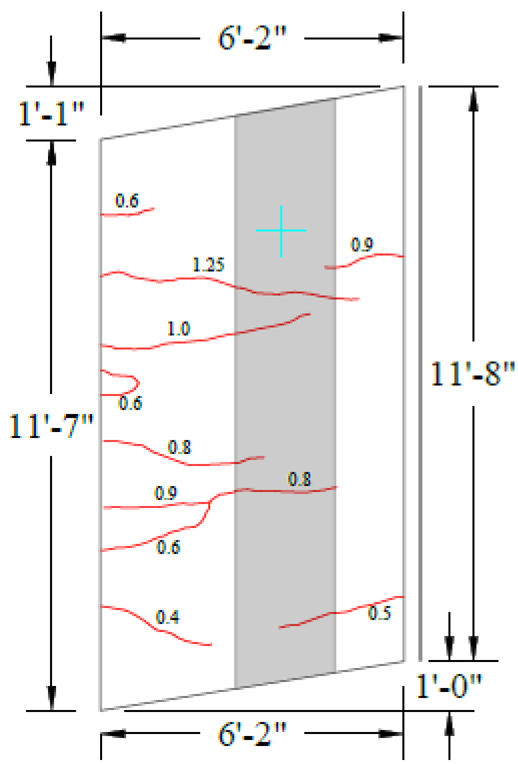

Figure B.2 Distress map for repair 1-3.

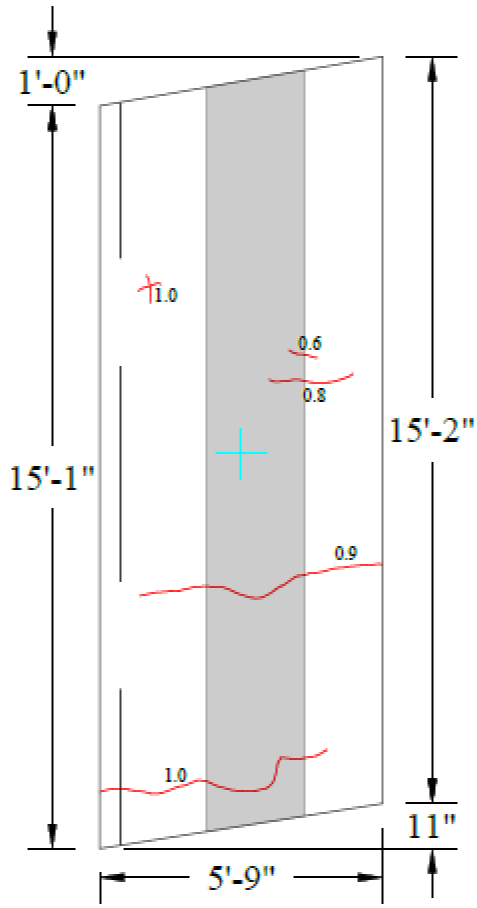

Figure B.3 Distress map for repair 1-10.

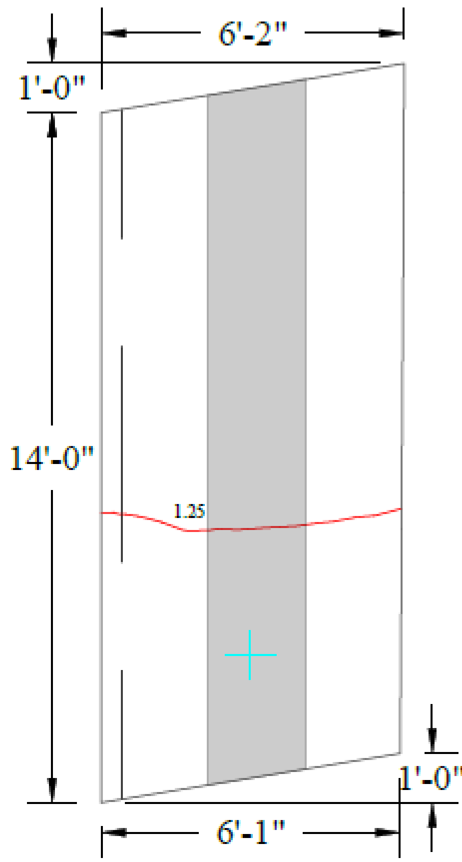

Figure B.4 Distress map for repair 1-13.

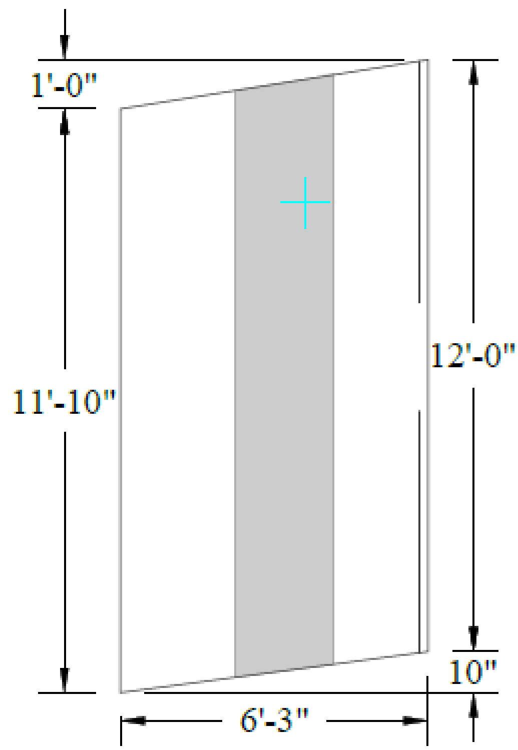

Figure B.5 Distress map for repair 2-1.

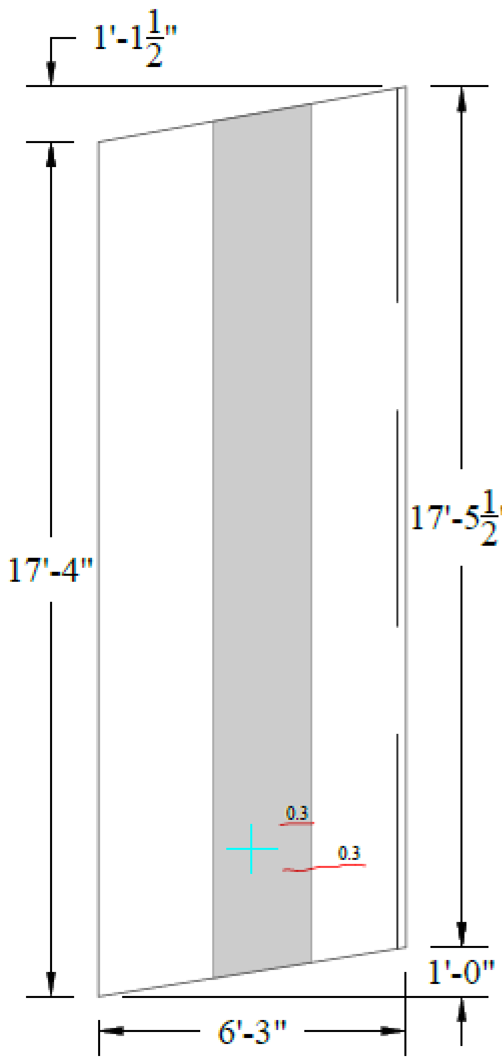

Figure B.6 Distress map for repair 2-2.

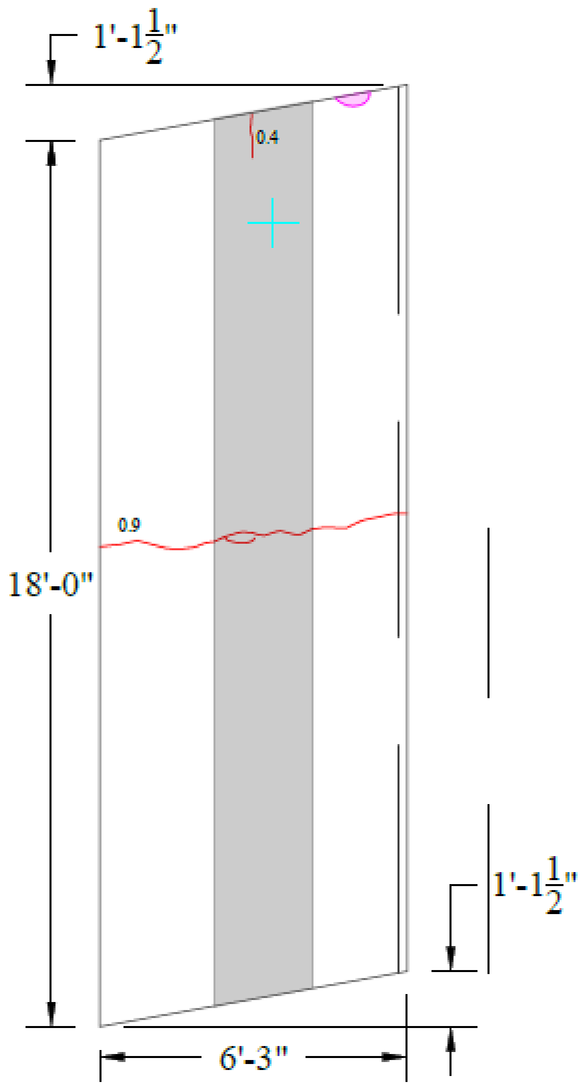

Figure B.7 Distress map for repair 2-3.

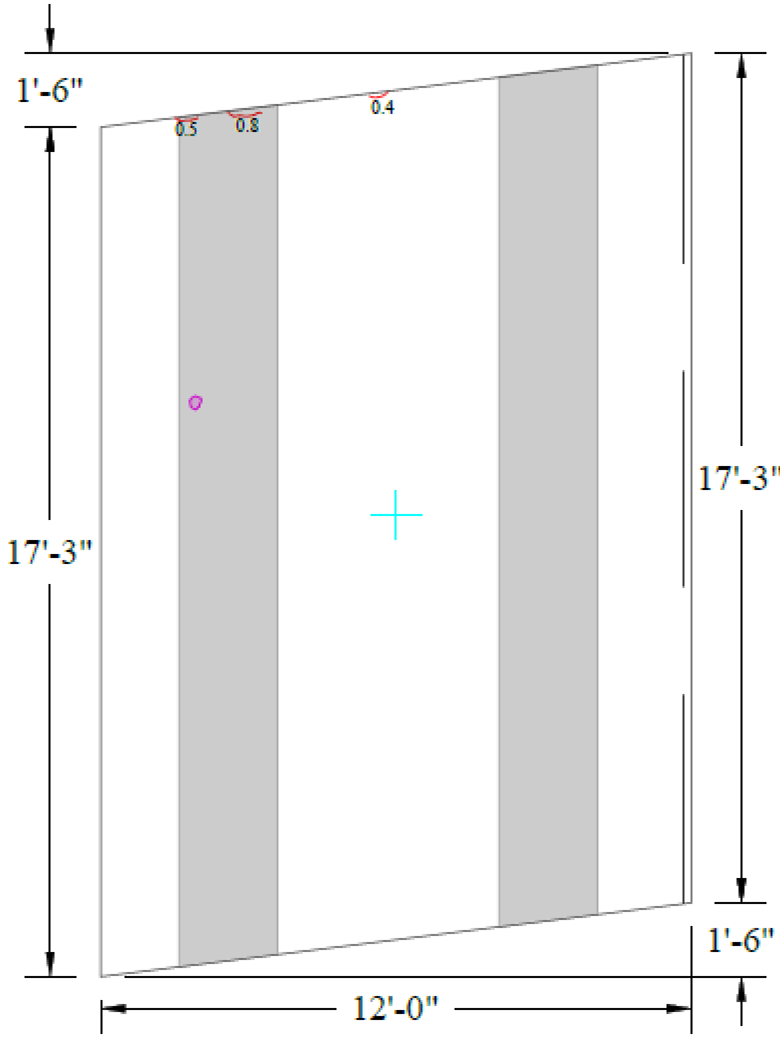

Figure B.8 Distress map for repair 2-4.

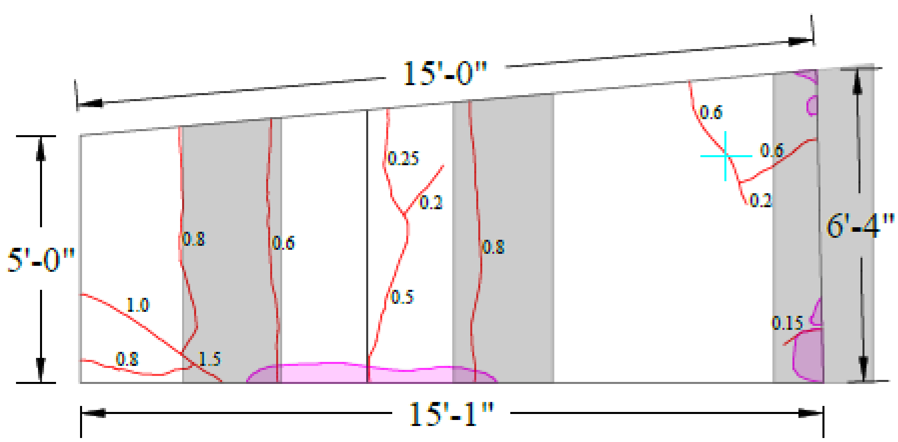

Figure B.9 Distress map for repair 3-1.

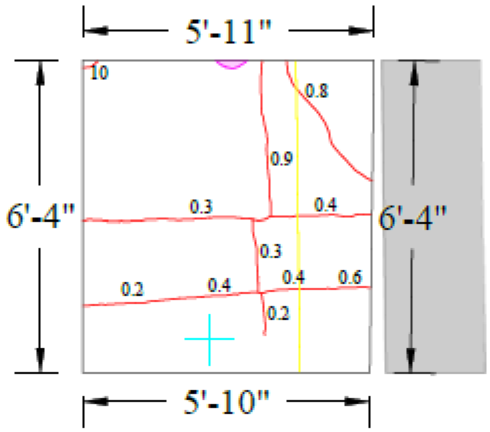

Figure B.10 Distress map for repair 3-2.

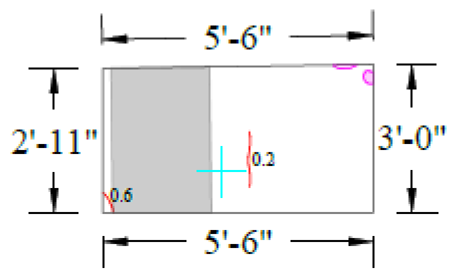

Figure B.11 Distress map for repair 3-3.

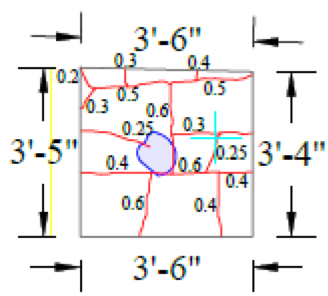

Figure B.12 Distress map for repair 4-1.

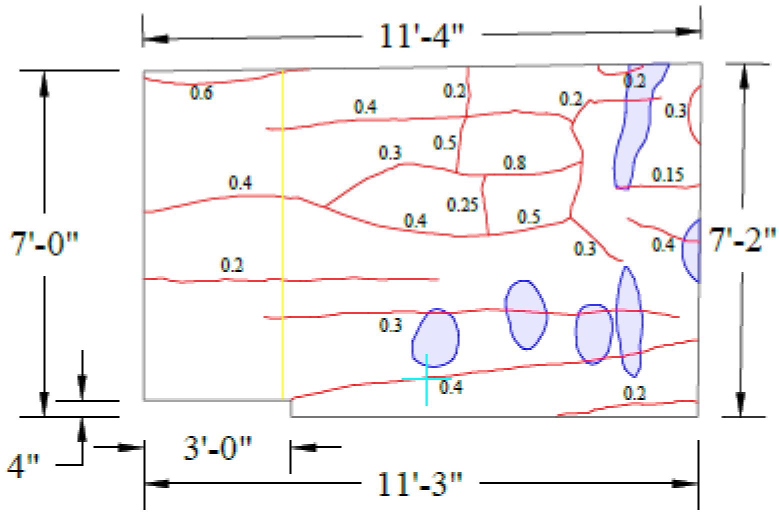

Figure B.13 Distress map for repair 4-11.

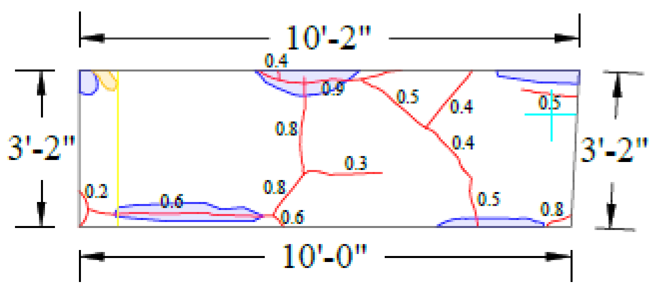

Figure B.14 Distress map for repair 4-19.

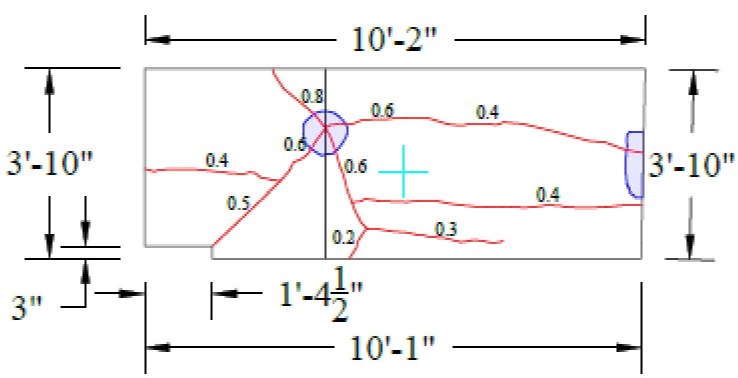

Figure B.15 Distress map for repair 4-24.

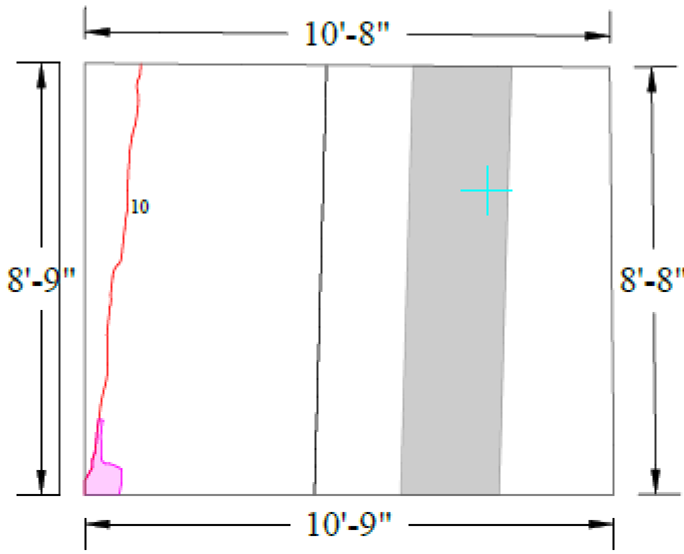

Figure B.16 Distress map for repair 5-1.

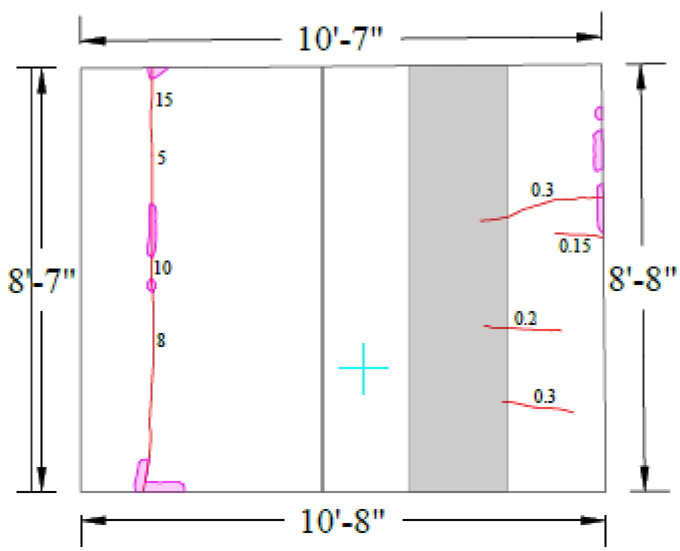

Figure B.17 Distress map for repair 5-2.

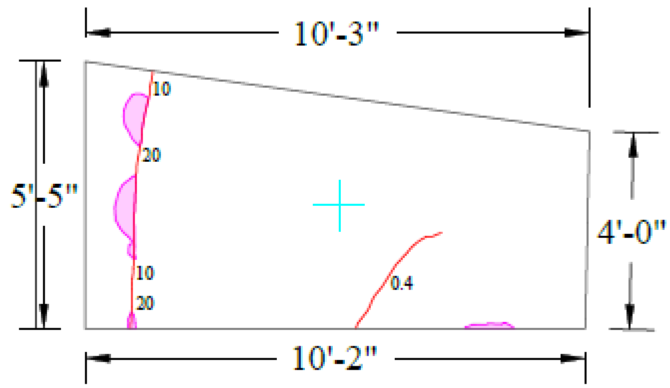

Figure B.18 Distress map for repair 5-3.

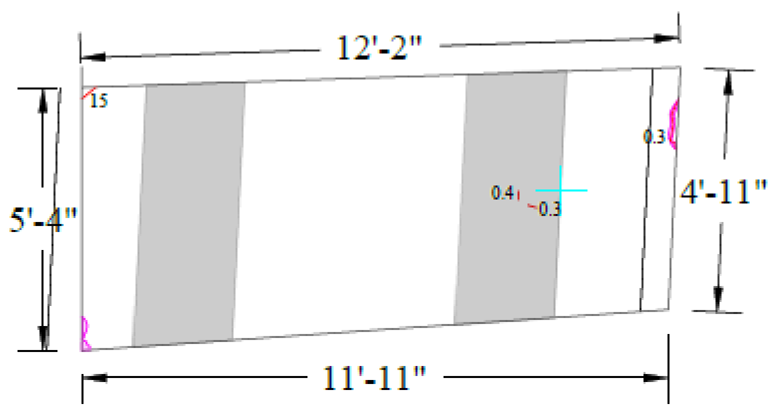

Figure B.19 Distress map for repair 6-3.

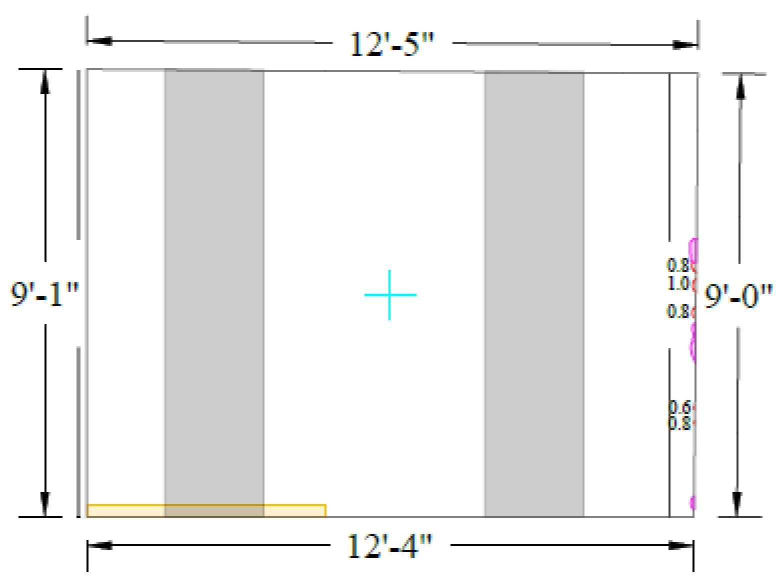

Figure B.20 Distress map for repair 6-13.

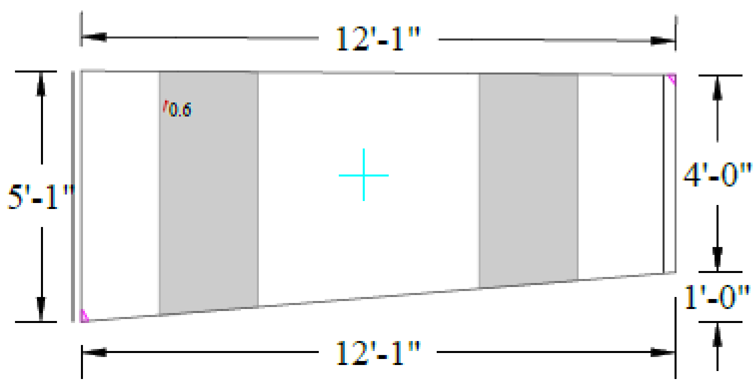

Figure B.21 Distress map for repair 6-17.

APPENDIX C: PHOTOGRAPHS OF EVALUATED REPAIRS

Figure C.1 Repair 1-3.

Figure C.2 Repair 1-10.

Figure C.3 Repair 1-13.

Figure C.4 Repair 2-1.

Figure C.5 Repair 2-2.

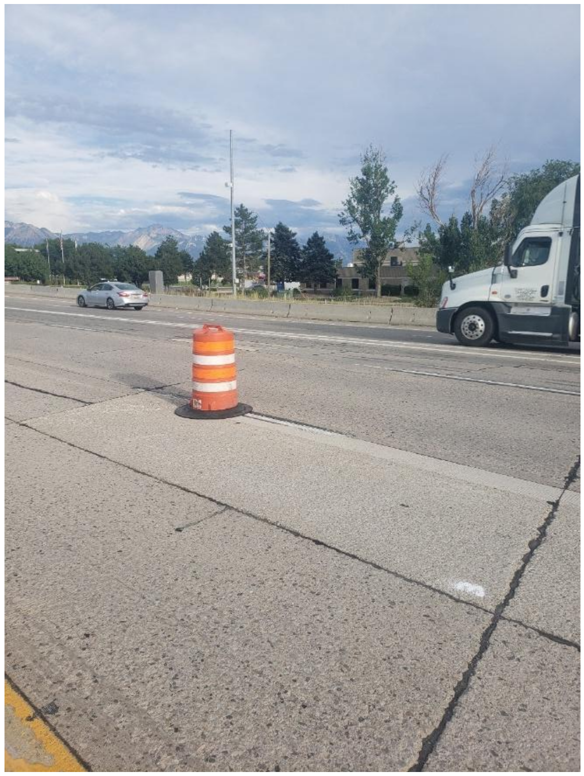

Figure C.6 Repair 2-3.

Figure C.7 Repair 2-4.

Figure C.8 Repair 3-1.

Figure C.9 Repair 3-2.

Figure C.10 Repair 3-3.

Figure C.11 Repair 4-1.

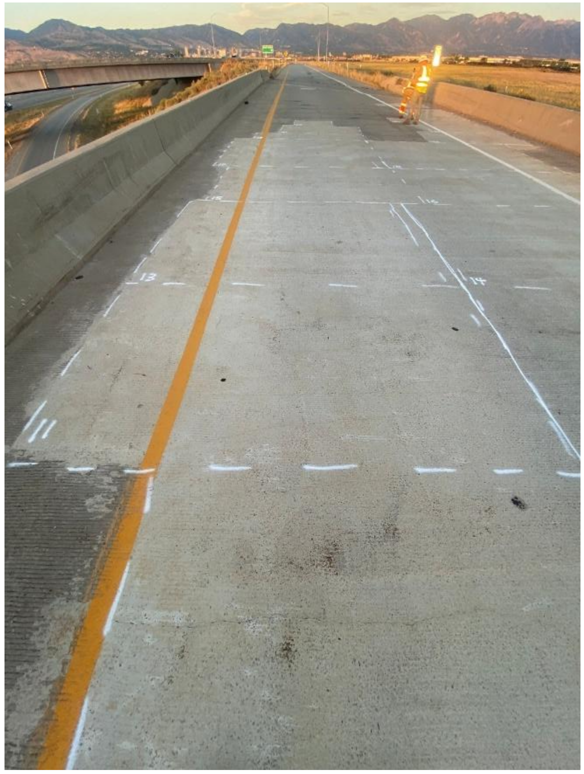

Figure C.12 Repair 4-11.

Figure C.13 Repair 4-19.

Figure C.14 Repair 4-24.

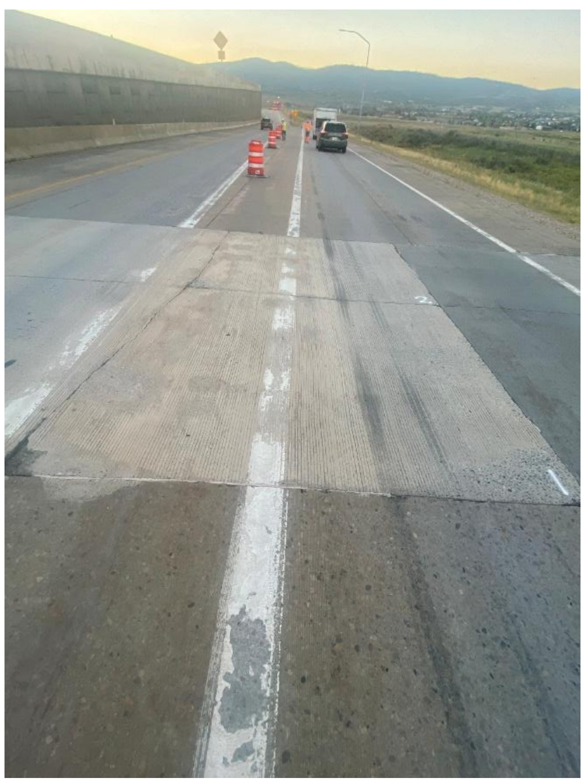

Figure C.15 Repair 5-1.

Figure C.16 Repair 5-2.

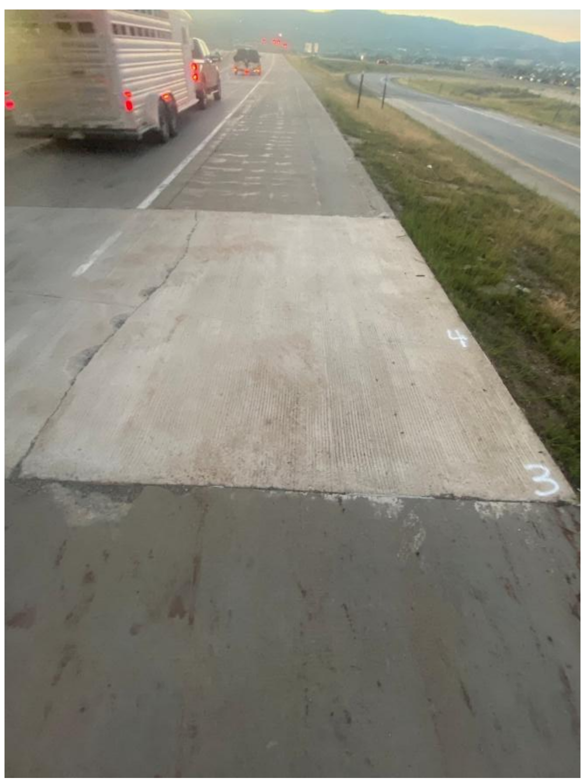

Figure C.17 Repair 5-3.

Figure C.18 Repair 6-3.

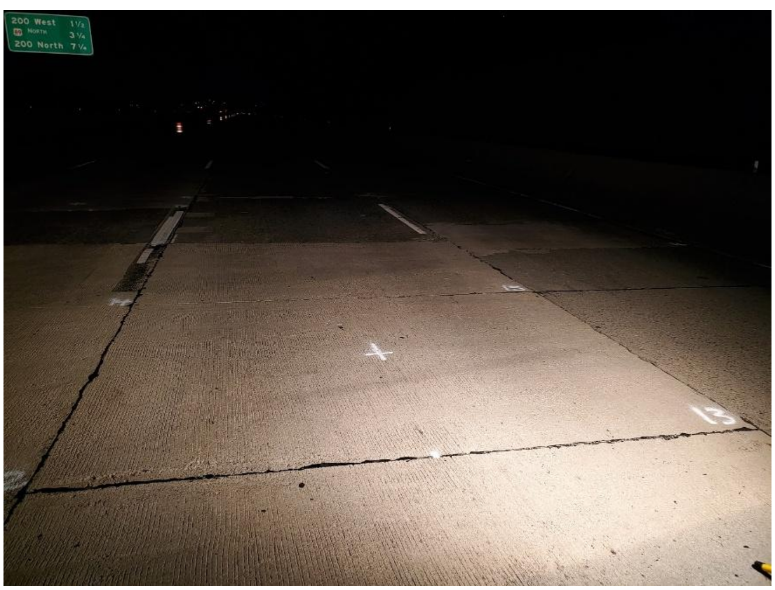

Figure C.19 Repair 6-13.

Figure C.20 Repair 6-17.

APPENDIX D: PHOTOGRAPHS OF CORE SAMPLES

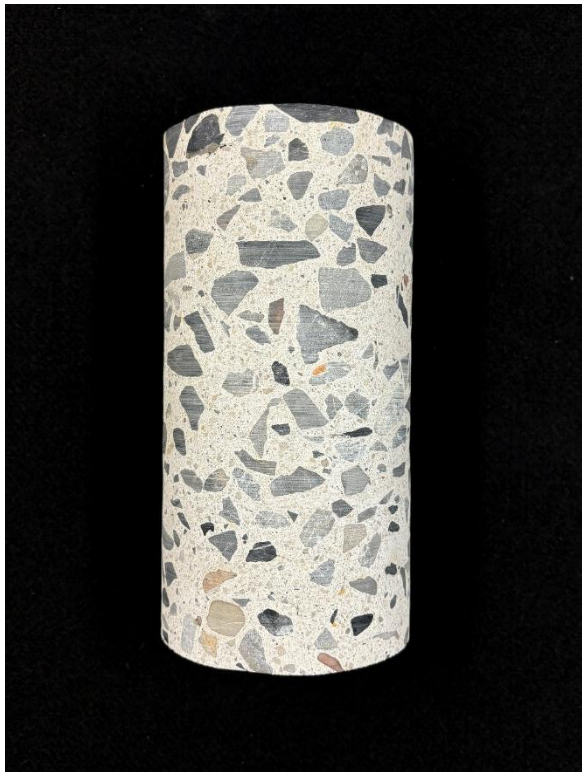

Figure D.1 Core 1-3.

Figure D.2 Core 1-10.

Figure D.3 Core 1-13.

Figure D.4 Core 2-1.

Figure D.5 Core 2-2.

Figure D.6 Core 2-3.

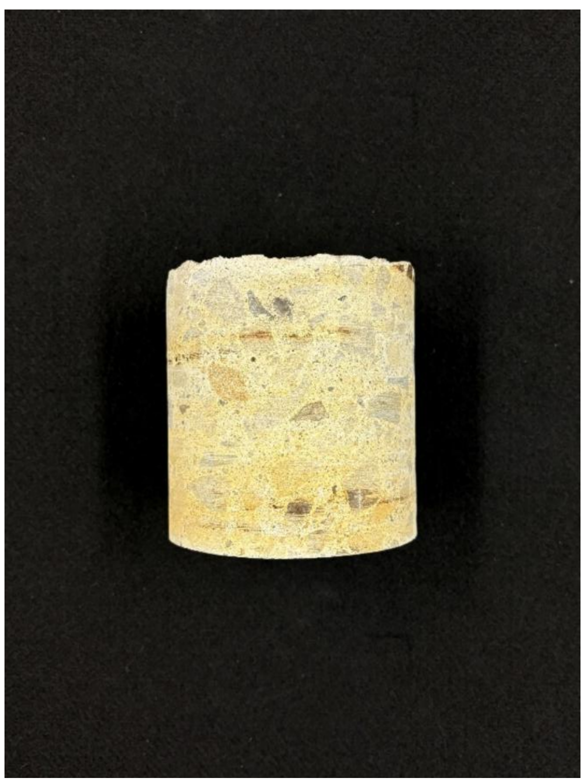

Figure D.7 Core 2-4.

Figure D.8 Core 3-1.

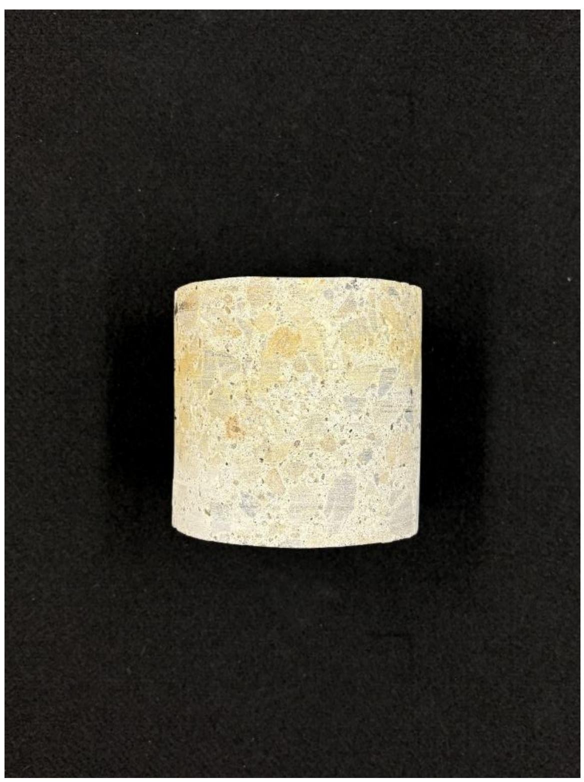

Figure D.9 Core 3-2.

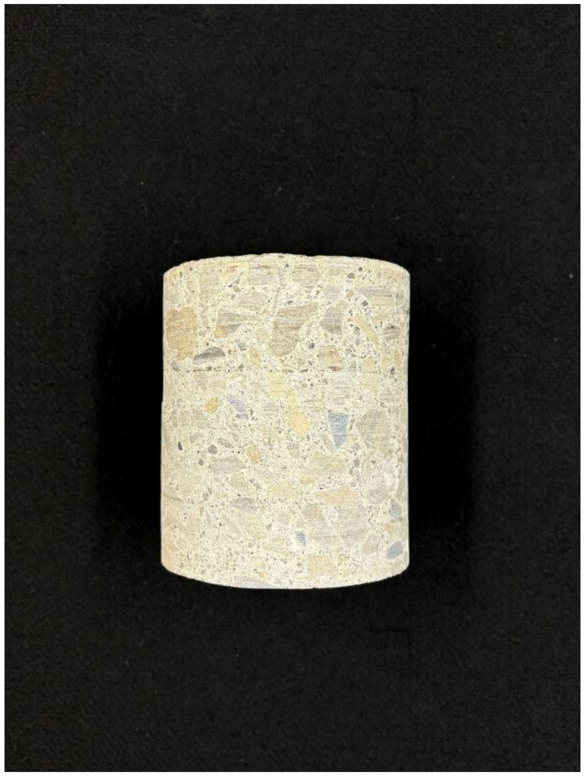

Figure D.10 Core 3-3.

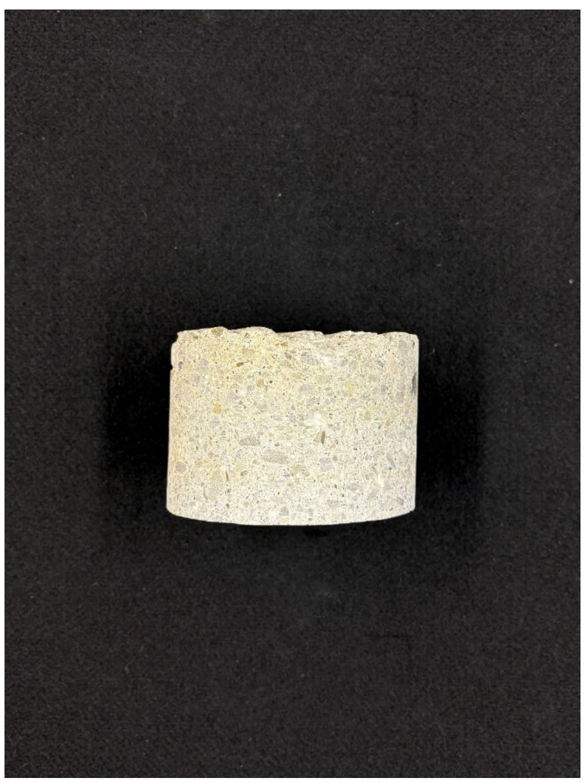

Figure D.11 Core 4-1-1.

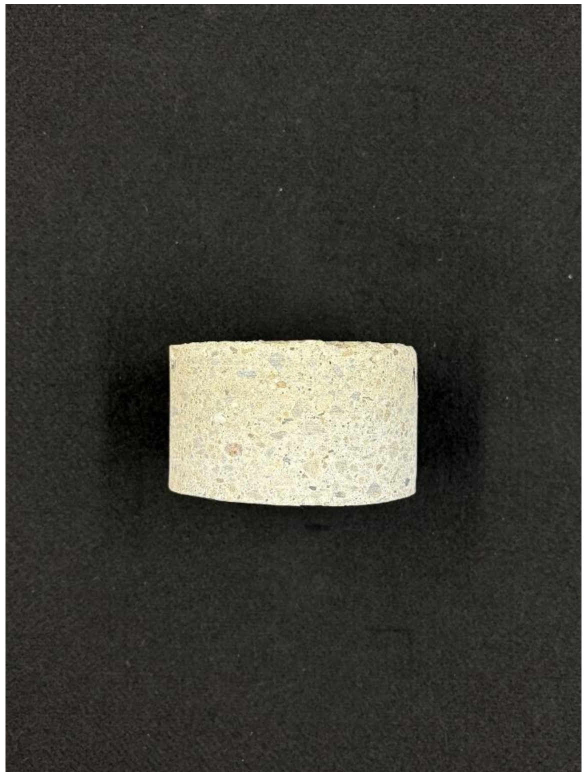

Figure D.12 Core 4-1-2.

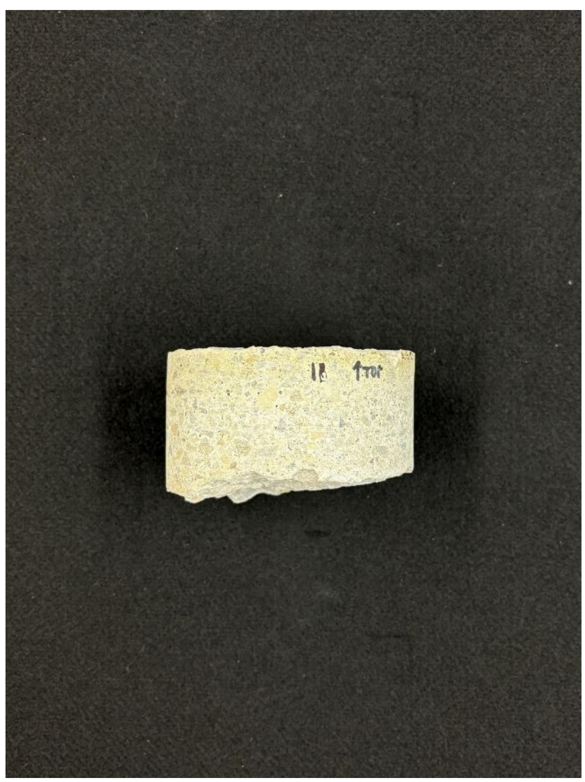

Figure D.13 Core 4-11.

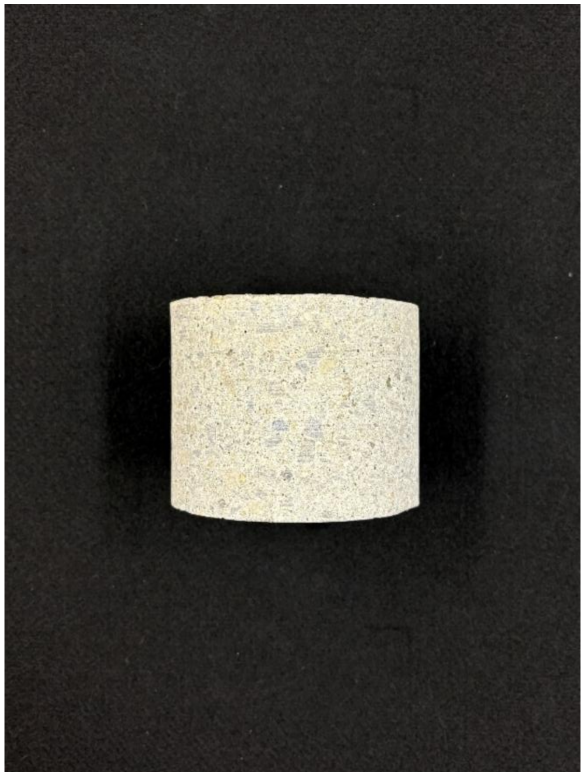

Figure D.14 Core 4-19.

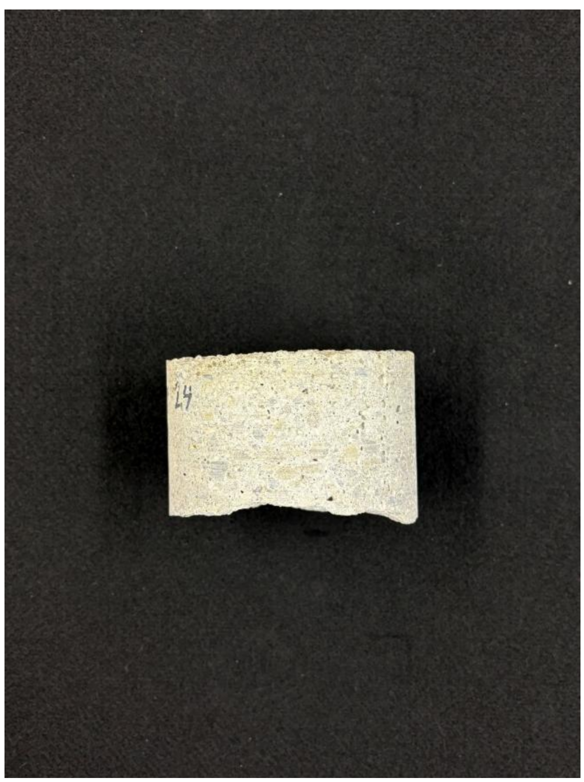

Figure D.15 Core 4-24.

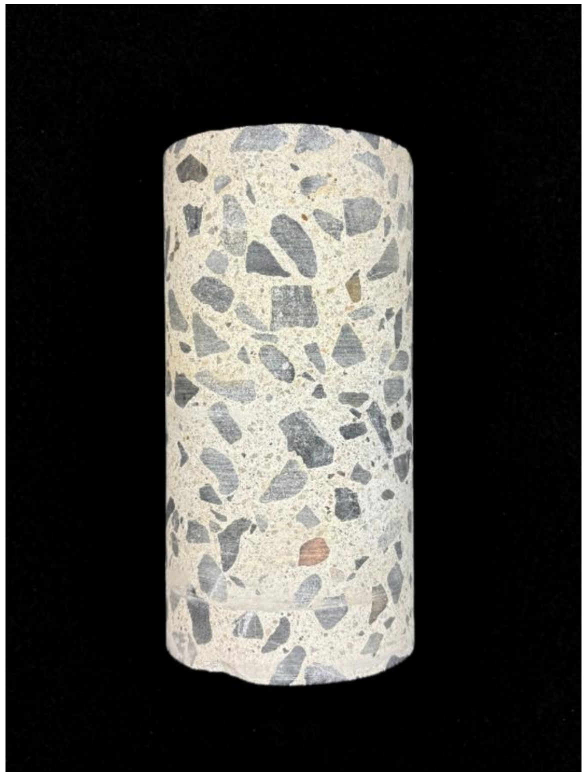

Figure D.16 Core 5-1.

Figure D.17 Core 5-2.

Figure D.18 Core 5-3.

Figure D.19 Core 6-3.

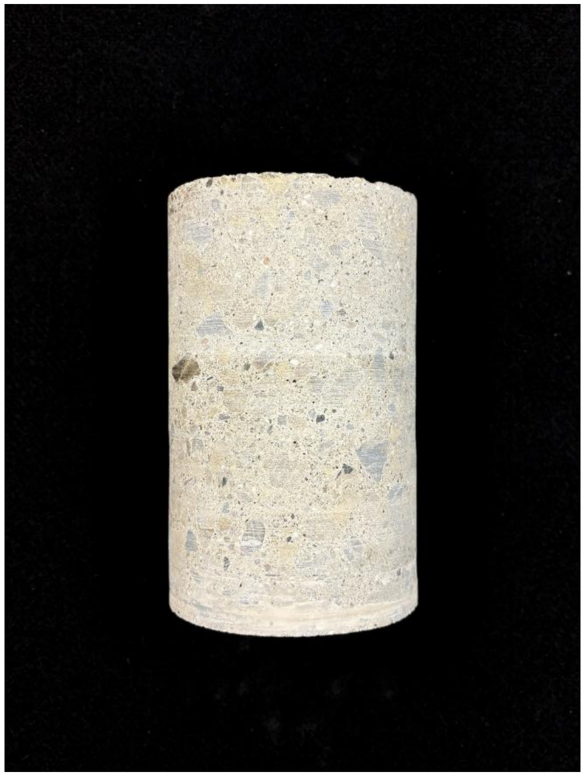

Figure D.20 Core 6-13.

Figure D.21 Core 6-17.

APPENDIX E: PHOTOGRAPHS FROM HARDENED AIR VOID ANALYSES

In Figures E.1 and E.2, the dashed red lines indicate the lower limit of the depth of analysis.

Figure E.1 Section of core 1-10 (1).

Figure E.2 Section of core 1-10 (2).

Figure E.3 Section of core 2-4 (1).

Figure E.4 Section of core 2-4 (2).

Figure E.5 Section of core 4-1-2 (1).

Figure E.6 Section of core 4-1-2 (2).

Figure E.7 Microscope image of core 1-10 (1).

Figure E.8 Microscope image of core 1-10 (2).

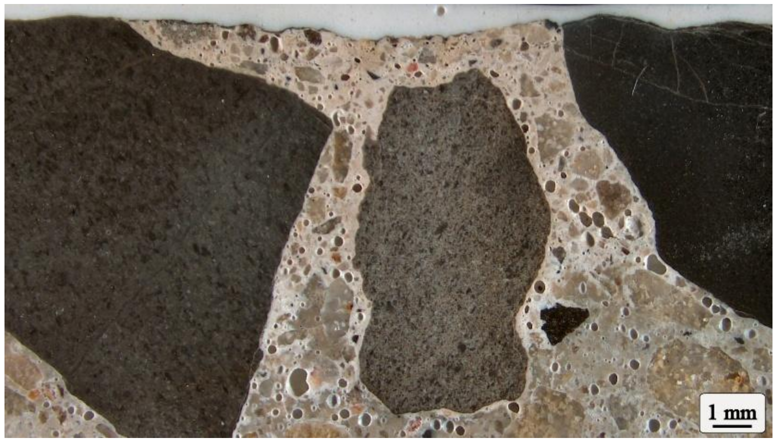

Figure E.9 Microscope image of core 1-10 (3).

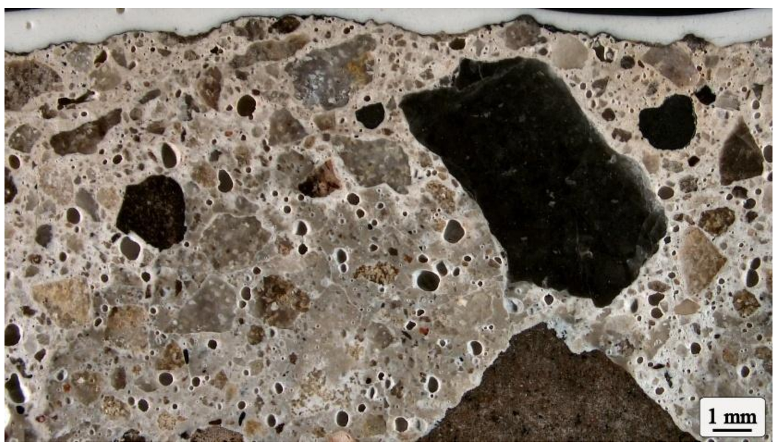

Figure E.10 Microscope image of core 1-10 (4).

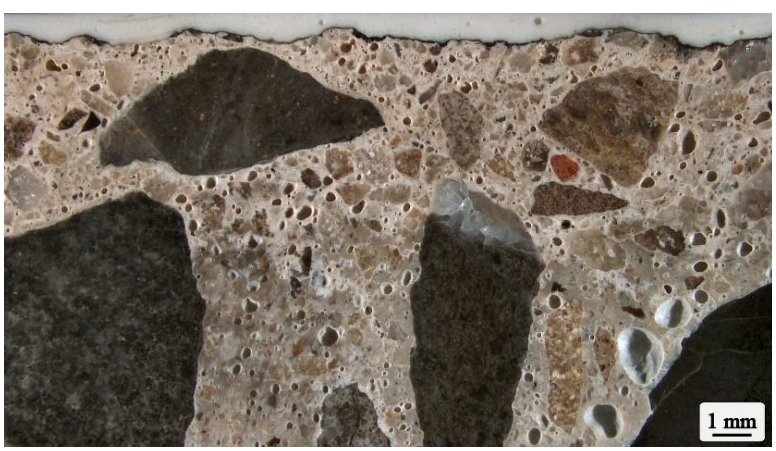

Figure E.11 Microscope image of core 1-10 (5).

Figure E.12 Microscope image of core 2-4 (1).

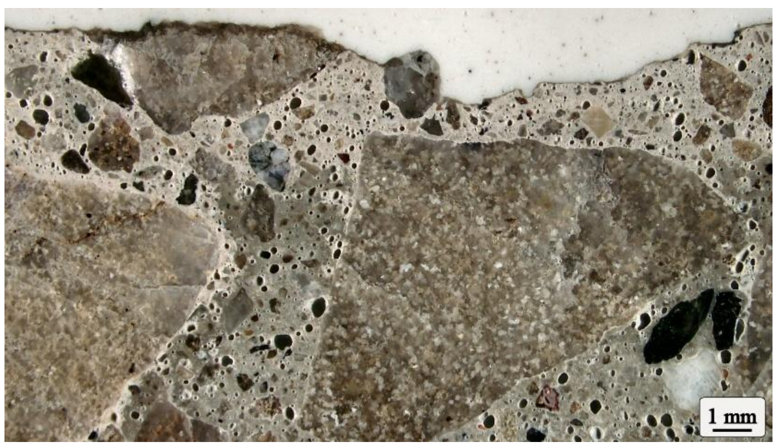

Figure E.13 Microscope image of core 2-4 (2).

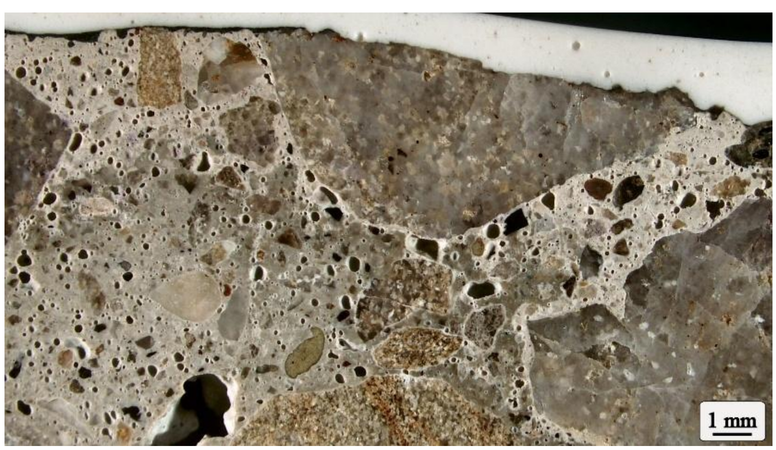

Figure E.14 Microscope image of core 2-4 (3).

Figure E.15 Microscope image of core 2-4 (4).

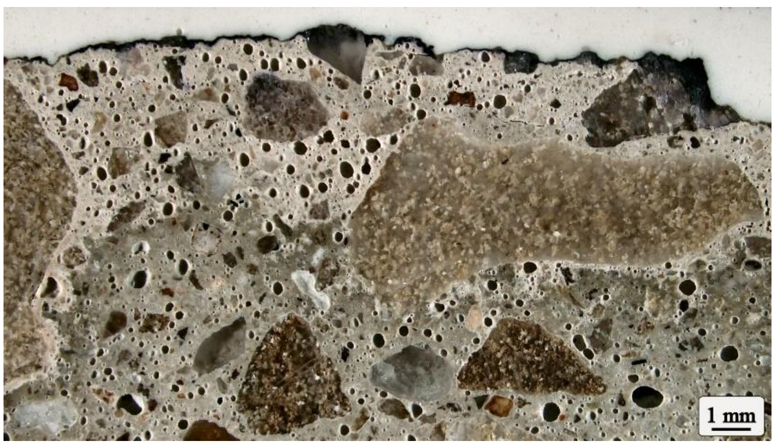

Figure E.16 Microscope image of core 2-4 (5).

Figure E.17 Microscope image of core 4-1-2 (1).

Figure E.18 Microscope image of core 4-1-2 (2).

Figure E.19 Microscope image of core 4-1-2 (3).

Figure E.20 Microscope image of core 4-1-2 (4).

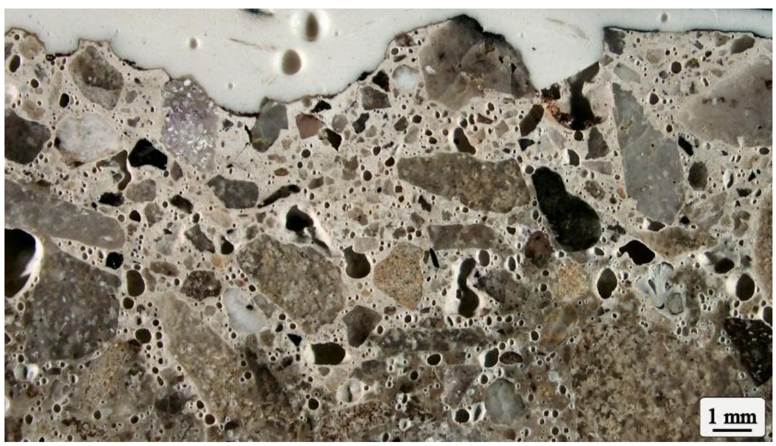

Figure E.21 Microscope image of core 4-1-2 (5).